Geosphere

Sea-level control of New Jersey margin architecture: Palynological evidence from Integrated Ocean Drilling Program Expedition 313

Francine M.G. McCarthy, Miriam E. Katz, Ulrich Kotthoff, James V. Browning, Kenneth G. Miller, Ryan Zanatta, Ross H. Williams, Matea Drljepan, Stephen P. Hesselbo, Christian J. Bjerrum and Gregory S. Mountain

Geosphere published online 23 October 2013;
doi: 10.1130/GES00853.1

Notes

Sea-level control of New Jersey margin architecture: Palynological evidence from Integrated Ocean Drilling Program Expedition 313

Francine M.G. McCarthy[1], Miriam E. Katz[2], Ulrich Kotthoff[3], James V. Browning[4], Kenneth G. Miller[4], Ryan Zanatta[1], Ross H. Williams[2], Matea Drljepan[1], Stephen P. Hesselbo[5], Christian J. Bjerrum[6], and Gregory S. Mountain[4]

[1]*Department of Earth Sciences, Brock University, St. Catharines, ONT L2S 3A1, Canada*
[2]*Department of Earth & Environmental Sciences, Rensselaer Polytechnic Institute, Troy, New York 12180, USA*
[3]*Institut für Geologie, Universität Hamburg, Bundesstrasse 55, 20146 Hamburg, Germany*
[4]*Department of Earth and Planetary Sciences, Rutgers University, Piscataway, New Jersey 08854, USA*
[5]*Camborne School of Mines, College of Engineering, Mathematics and Physical Sciences, University of Exeter, Penryn Campus, Penryn, Cornwall TR10 9EZ, UK*
[6]*Nordic Centre for Earth Evolution (NordCEE) and Department of Geosciences and Natural Resource Management, Øster Voldgade 10, DK-1350, Copenhagen K, Denmark*

ABSTRACT

Integrated Ocean Drilling Program Expedition 313 recovered Miocene sequences at Holes M0027A and M0029A on the New Jersey shallow shelf that contain a characteristic acid-resistant organic component. The palynofacies within each sequence reflects variations in terrigenous versus authigenic flux through the Miocene that are associated with sea-level change. Very high ratios of terrigenous versus marine palynomorphs and of oxidation-resistant versus susceptible dinocysts are associated with seismic sequence boundaries, consistent with their interpretation as sequence-bounding unconformities generated at times of low sea level. Comparison of palynological distance from shoreline estimates with paleodepth estimates derived from foraminiferal data allows relative sea level to be reconstructed at both sites. Ages assigned using dinocyst biostratigraphy are consistent with other chronostratigraphic indicators allowing sequence boundaries to be correlated with Miocene oxygen isotope (Mi) events. Paleoclimatic evidence from the pollen record supports the global climate changes seen in the oxygen isotope data. Although chronological control is relatively crude, Milankovitch-scale periodicity is suggested for parasequences visible in thick sequences deposited in relatively deep water where substantial accommodation existed, such as during the early Langhian at Site 29 (Middle Miocene Climatic Optimum). Palynological analysis thus supports the long-held hypothesis that glacioeustasy is a dominant process controlling the architecture of continental margins.

INTRODUCTION

Integrated Ocean Drilling Program Expedition 313 to the New Jersey Shallow Shelf

The New Jersey margin is ideally suited to study the response of continental margin architecture to Oligocene–Miocene icehouse sea-level fluctuations (Mountain et al., 2010). Integrated Ocean Drilling Program (IODP) Expedition 313 provided an opportunity to apply a multiproxy approach to refining the application of palynology to sequence stratigraphic studies. In 1998, Ocean Drilling Program (ODP) Leg 174A attempted to core the outer New Jersey (USA) shelf, but recovery (particularly of the sand-rich Miocene section) was patchy, so the shipboard party (Austin et al., 1998) was forced to focus on the Quaternary of the uppermost slope. Drilling by onshore ODP Legs 150X and 174AX successfully recovered Late Cretaceous to Holocene sequences from sites on the Atlantic coastal plain (summaries in Miller, 2002; Miller et al., 2005) that provide the material to reconstruct sea level on the New Jersey margin and relate the fluctuations to global sea-level change (e.g., Miller et al., 2005). There remained a gap between the coastal plain and the outer shelf, making correlation difficult until the New Jersey shallow shelf was finally drilled between 30 April and 17 July 2009 by IODP Expedition 313, filling the critical gap in the transect of coreholes between the New Jersey coastal plain (ODP Legs 150X and 174AX) and the continental slope (ODP Legs 150 and 174A) (Fig. 1).

There were 15 unconformity-bounded sequences identified within the Miocene during Expedition 313 (Mountain et al., 2010). Seismic sequence boundaries were identified based on reflector terminations (onlap, downlap, erosional truncation, and toplap) on multichannel seismic profiles obtained on R/V *Ewing* cruise Ew9009, R/V *Oceanus* cruise Oc270, and R/V *Cape Hatteras* cruise Ch0698 (Fig. 1; Monteverde et al., 2008; Monteverde, 2008; Mountain et al., 2010). Sequence boundaries were identified in the Expedition 313 cores on the basis of physical stratigraphy and age breaks (Mountain et al., 2010; Browning et al., 2013; Miller et al., 2013a) based on the following criteria: (1) irregular contacts, with as much as 5 cm of relief on a 6.2-cm-diameter core; (2) reworking, including rip-up clasts found above the contact; (3) intense bioturbation, including burrows filled with overlying material; (4) major lithofacies shifts and changes in stacking pattern; (5) gamma-ray increases associated with changes from low radioactivity sands below to "hotter" (high radioactivity) clays above, glauconite immediately above sequence boundaries, and/or marine omission surfaces (e.g., with high U/Th scavenging); (6) shell lags above the contact; and (7) age breaks indicated by Sr isotope stratigraphy or biostratigraphy. A velocity versus depth function was used to make initial seismic-core correlations of seismic sequence boundaries to core surfaces identified from visual

Geosphere; December 2013; v. 9; no. 6; doi:10.1130/GES00853.1; 11 figures; 6 tables; 2 supplemental tables.
Received 4 August 2012 ♦ Revision received 31 August 2013 ♦ Accepted 2 October 2013 ♦ Published online 23 October 2013

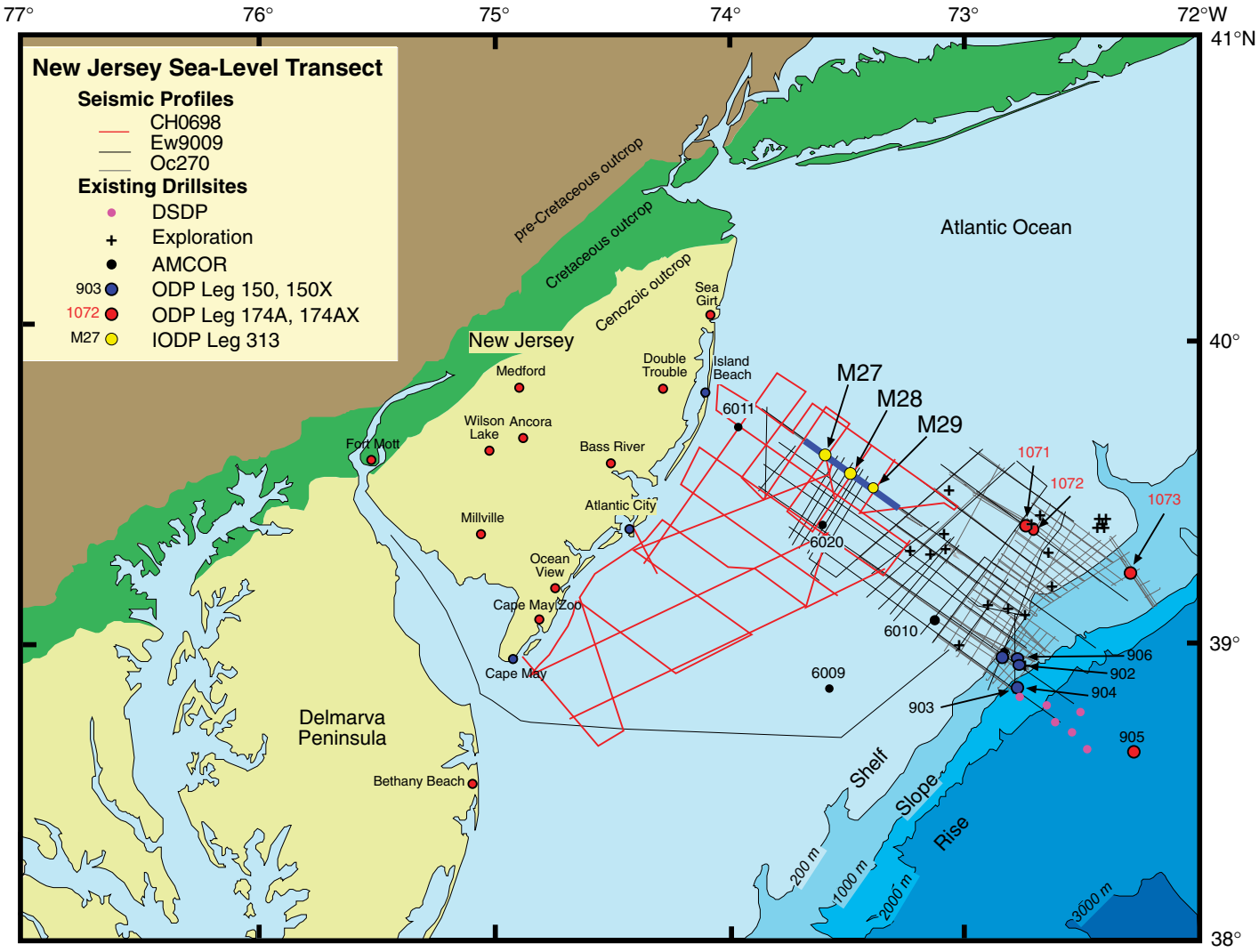

Figure 1. Generalized bathymetric and location map of the New Jersey/Mid Atlantic Margin transect showing three generations of multichannel seismic (MCS) data (R/V *Ewing* cruise Ew9009, R/V *Oceanus* cruise Oc270, and R/V *Cape Hatteras* cruise Ch0698) acquired before Expedition 313, as well as onshore coreholes and offshore coreholes drilled by AMCOR (Atlantic Margin Coring Project), ODP (Ocean Drilling Program), and IODP (Integrated Ocean Drilling Program). DSDP—Deep Sea Drilling Project. Palynomorphs were analyzed from Sites M27 and M29 at the proximal and distal ends of the IODP Expedition 313 transect.

evidence (core descriptions and photographs) and log data (Mountain et al., 2010; Mountain and Monteverde, 2012; Miller et al., 2013a). Synthetic seismograms from Sites M27A and M29A (Mountain and Monteverde, 2012) provide a check on seismic-core correlations and predicted depths of seismic sequence boundaries. The resultant seismic-core-log correlations (summarized in Miller et al., 2013a) were used to place the sequence boundaries in this study. A chronology was developed based on calcareous nannofossil, diatom, dinoflagellate cyst, and planktonic foraminiferal data together with Sr isotope analyses of mollusc shells and foraminifers that allowed correlation with the global record of eustasy (see Browning et al., 2013).

Sea-Level–Sensitive Palynological Proxies

Several studies have used palynomorphs in sequence stratigraphic studies, recognizing their significance as sedimentary particles having provenance and history that can be much more comprehensively identified than those of the siliciclastic particles with which they are deposited (Eshet et al., 1988; Habib and Miller, 1989; Gregory and Hart, 1992; Wood and Gorin, 1998; McCarthy and Gostlin, 2000; McCarthy et al., 2003; Oboh-Ikuenobe et al., 2005). All of these studies demonstrated that the palynological signature of a continental margin is the product of the initial environmental conditions at the depositional setting together with taphonomic skewing of that record due to differential transport and preservation of palynomorphs (in addition to the biostratigraphically useful evolution and extinction events). The basic concept is that acid-resistant organic material from land (e.g., phytoclasts, fungal spores, pollen, and embryophyte spores) is progressively sorted and degraded with increasing distance from the shoreline because of a progressively decreasing energy gradient. In contrast, autochthonous marine material is preferentially degraded in the higher energy proximal settings, but is preserved well in deeper water settings as long as the burial rate is relatively high (Traverse, 1994; Tyson 1995).

In this paper sea-level–dependent aspects of the palynological record of Holes M0027A and

M0029A (herein 27A and 29A) are examined in light of one of the main goals of IODP Expedition 313, i.e., to assess the role of sea level on continental margin architecture (Mountain et al., 2010). Estimates of the proximity to the shoreline inferred from the palynological record are compared with estimates of paleo–water depth derived from benthic foraminiferal data, which have long been the basis for sea-level reconstruction (e.g., Miller et al., 1997; Katz et al., 2003). Previous comparisons of palynologically derived distance to shoreline estimates and benthic foraminiferal biofacies-based paleobathymetry in Pleistocene sediments from ODP Hole 1072A proved successful (Katz et al., 2003; McCarthy et al., 2003).

Comparison of the palynological record (which represents the allochthonous pollen flux together with the in situ planktonic algal record, thus providing a proxy of terrigenous flux to marine environments) with the benthic foraminiferal record (which provides estimates of paleobathymetry) allows some of the complexity associated with the palynological response to sea-level change to be resolved, and a robust signal is obtained when all of the proxies are integrated and interpreted to record the same paleoenvironmental parameters. This multiproxy approach also highlights different aspects of variations in relative sea level that are recorded by the different microfossil groups. A shelf with a steep gradient, for example, could have proximal conditions (recorded by a strong dominance of terrestrial microfossils) together with outer neritic water depths (inferred from foraminiferal assemblages), whereas a shelf with a very gentle gradient could have distal settings, resulting in a lower ratio of terrestrial versus marine microfossils in sediments containing a benthic foraminiferal assemblage, reflecting inner neritic water depths. In addition, beyond the shelf break, downslope mass wasting (which is most pronounced at times of lowered sea level; cf. McCarthy et al., 2003, 2004a) can produce palynomorph assemblages very rich in pollen and embryophyte spores in relative deep water. The multiproxy data and the very good age resolution available from IODP Expedition 313 allow us to assess existing models and to infer the relationship between sea level and the sedimentation of organic particles on the New Jersey margin during the early Aquitanian to early Serravallian.

METHODS

Samples (5 cm^3) were processed for palynological analysis at Brock University (St. Catharines, Canada) using standard techniques, including disaggregation using warm, dilute (0.02%) sodium hexametaphosphate, and dissolution of carbonate and silicate minerals using weak (10%) HCl and concentrated HF, respectively. Samples were centrifuged and rinsed with distilled water between each ~1 h step. Samples were sieved twice through Nitex mesh to retain the >15 µm fraction, once after the weak sodium hexametaphosphate treatment to get rid of the majority of the resistant clays, and more thoroughly following the HF treatment to get rid of any remaining clays as well as fine organic matter that can obstruct palynomorph identification. A tablet containing 10,850 ± 200 *Lycopodium clavatum* spores was introduced during HCl treatment in order to allow estimates of marine and terrestrial palynomorph concentration relative to the exotic spores (as described by Stockmarr, 1971). Samples were mounted on glass slides using glycerine jelly and palynomorphs were counted at 400× magnification, with specimens examined under oil immersion at 1000× for verification where necessary. The identification of palynomorphs was hampered in many samples by the growth of pyrite, indicating that reducing conditions prevailed in the depositional environment. The abundance of dinoflagellate cysts and amorphous organic matter (AOM) in these pyrite-rich samples records that reducing conditions were associated with distal/outer neritic conditions. In some samples, AOM was so common that it obscured some palynomorphs, preventing identification. In Serravallian sediments at the more neritic Site 27, and in most samples at sequence boundaries, marine palynomorphs were vastly outnumbered by terrestrial palynomorphs and terrigenous organic matter, so that several slides had to be examined. Nonetheless, nearly all Miocene samples processed contained sufficient reasonably well preserved palynomorphs to allow assessment of age and paleoenvironment; the exception was sandy sediments that make up the upper part of sequence m5.8 and sequence m5.47 in Hole 27A.

Photographs of common and age-diagnostic dinocyst taxa were taken at 1000× using oil immersion. The dinocyst data (raw counts in Supplemental Tables 1[1] and 2[2]) are presented semiquantitatively as relative abundances (rare < 5%, common 5%–20%, abundant > 20%) based on minimum counts of 35 cysts, although counts normally exceed 60 cysts. Ages were assigned to samples using the dinoflagellate (DN) zones of de Verteuil and Norris (1996) (Fig. 2), although more recent dinocyst studies, most notably the North Sea zonations of Dybkjær and Piasecki (2008, 2010) were also useful in assigning ages and characterizing sequences according to their palynological content. Useful datums calibrated to the Gradstein et al. (2004) time scale (as discussed in Browning et al., 2013) in Holes 27A and 29A are listed in Tables 1 and 2.

The degree of terrigenous versus marine flux is illustrated by the ratio of terrestrial palynomorphs (T, pollen + embryophyte spores) versus marine palynomorphs (M, dinocysts + acritarchs), i.e., T:M (referred to as P:D [pollen versus dinocysts] in McCarthy and Mudie [1998] and McCarthy et al. [2003, 2004a, 2004b]). Minimum counts of 200 palynomorphs were employed to generate ratios of terrestrial versus marine palynomorphs (Tables 3 and 4). Foraminiferal linings were not included in the total marine palynomorph sum because coastal and inner neritic benthics are as likely to produce acid-resistant linings as are middle to outer neritic taxa, and we are attempting to gauge sea level and terrigenous flux.

The T:M ratio illustrates the degree of terrigenous flux to the marine environment, representing the rapid settling of most pollen grains from the atmosphere and within the water column against an irregular pattern of algal productivity in surface waters (Mudie and McCarthy, 1994; McCarthy et al., 2003). A similar index is given by the ratio of two major end members of palynofacies classification: the allochthonous terrestrially derived phytoclasts (Ph) and authigenic marine AOM , i.e., Ph:AOM. Palynofacies identification follows Batten (1996), and the data are provided as a robust ratio of the terrigenous and marine end members (Figs. 3–5; Table 5). The Ph:AOM ratio primarily reflects taphonomic effects, e.g., the transportation of terrigenous organic matter relative to sea-surface productivity, and the ultimate preservation of that organic matter in the sediment. Distance from the shoreline is also reflected by the ratio of nonsaccate (primarily angiosperm/hardwood tree) versus bisaccate (conifer) pollen grains (nonsac:bisac; Figs. 3 and 4; Table 6), reflecting the gradual settling of heavier, less aerodynamic and hydrodynamic angiosperm grains (Mudie and McCarthy, 1994, McCarthy et al., 2003). Distal pollen assemblages thus tend to be greatly enriched in bisaccate conifer pollen with sacs adapted to float long distances in air or water.

The ratio of cysts of primarily coastal to inner neritic dinoflagellate taxa relative to those of

[1]Supplemental Table 1. Relative abundance and raw counts, Hole 27A. If you are viewing the PDF of this paper or reading it offline, please visit http://dx.doi.org/10.1130/GES00853.S1 or the full-text article on www.gsapubs.org to view Supplemental Table 1.

[2]Supplemental Table 2. Relative abundance and raw counts, Hole 29A. If you are viewing the PDF of this paper or reading it offline, please visit http://dx.doi.org/10.1130/GES00853.S2 or the full-text article on www.gsapubs.org to view Supplemental Table 2.

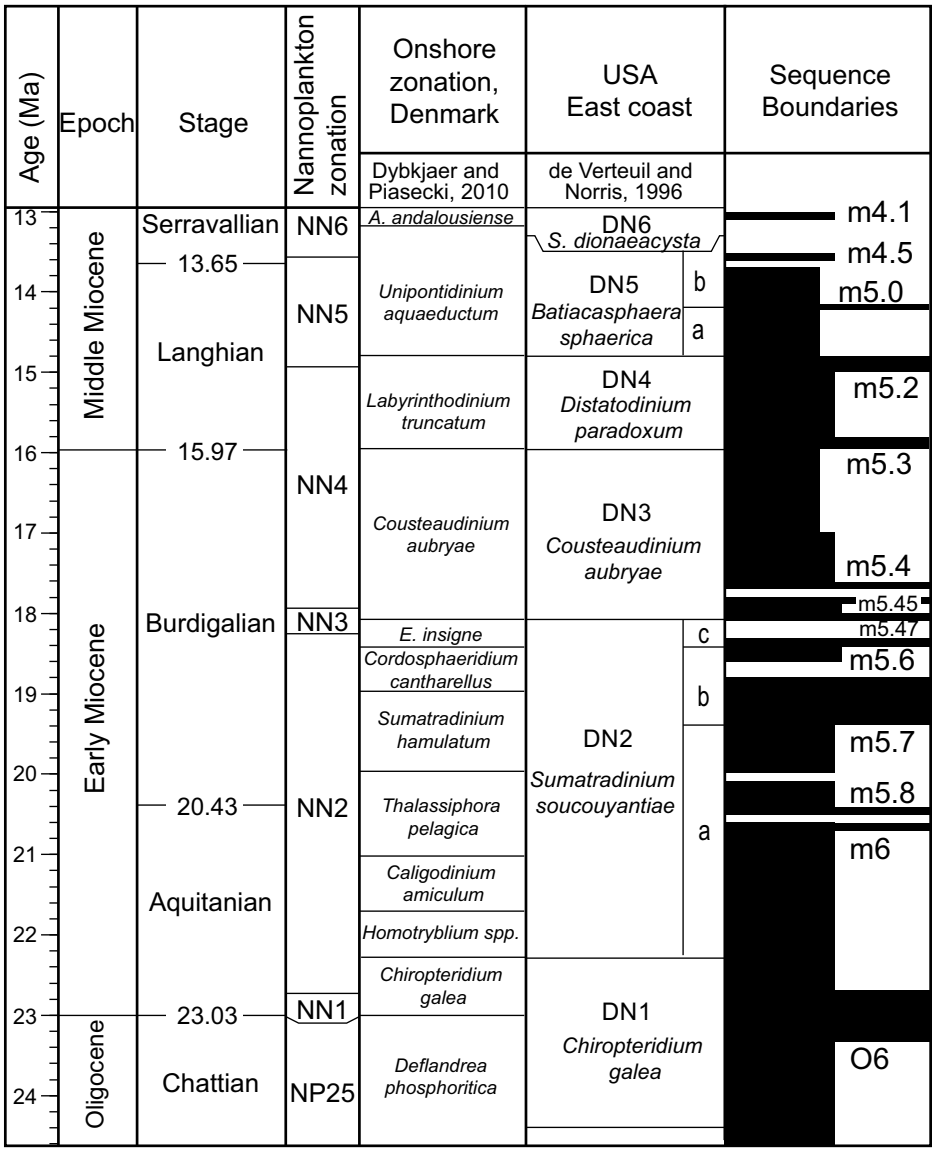

Figure 2. The dinocyst stratigraphy of de Verteuil and Norris (1996) allows ages to be assigned to Miocene sequences recovered from the New Jersey shelf and to sequence boundaries (unnamed–m4.1) that bound them. Dinoflagellate zone (DN) DN5 has been subdivided into subzones DN5a and DN5b, with the boundary between the subzones based on the lowest occurrence (LO) of *Habibacysta tectata*, which generally coincides with the highest consistent occurrence of *Apteodinium tectatum*, as reported by de Verteuil and Norris (1996). Subzones DN2a, DN2b, and DN2c are based on the highest occurrence (HO) of *Caligodinium amiculum*, *Cordosphaeridium cantharellum*, and *Exochosphaeridium insigne*, respectively. Also shown is the zonation of Dybkjær and Piasecki (2010) for the onshore sequences in Denmark, as well as the calcareous nannofossil zonation of Martini (1971). All are calibrated against the Gradstein et al. (2004) time scale, as discussed in Browning et al. (2013). The ages of sequence boundaries are constrained by the multiple chronostratigraphic proxies discussed in Browning et al. (2013). The thinner lines indicate the preferred and/or more constrained ages based on the dinocyst assemblages. A. andalousiense—Achomosphaera andalousiense; E. insigne—Exochosphaeridium insigne; S. dionaeacysta—Selenopemphix dionaeacysta.

primarily outer neritic and oceanic taxa is an additional indicator of distance to shoreline. The long-ranging so-called "round brown" *Brigantedinium* spp., associated with coastal to inner neritic environments or upwelling regions, i.e., regions with high nutrient availability (Rochon et al., 1999), are common to abundant in most samples from the New Jersey shallow shelf sites. These protoperidinioid cysts typically have a strong effect on the ratio of gonyaulacoid cysts (G; produced by autotrophic dinoflagellates and generally more abundant seaward of the inner shelf; see McCarthy et al., 2003) versus protoperidinioid cysts (P; produced by heterotrophic dinoflagellates and generally more abundant in coastal and inner neritic environments). G:P ratios (Figs. 3 and 4; Tables 3 and 4) thus provide another, relatively crude measure of the offshore environmental gradient; however, G:P is also high in distal settings where bottom waters are well oxygenated and the rate of burial is low, because postdepositional degradation selectively affects protoperidinioid cysts (Zonneveld et al., 1997; Hopkins and McCarthy, 2002; McCarthy et al., 2004a, 2004b; Versteegh and Zonneveld, 2002). The labile *Brigantedinium*-type cysts are especially vulnerable to early diagenetic aerobic degradation, while most gonyaulacoid taxa are highly resistant (Zonneveld et al., 2001, 2008; Versteegh and Zonneveld, 2002), so the G:P ratio referred to here also retains a taphonomic signature in addition to reflecting ecology. Sequence-bounding unconformities were found to be typically characterized by very high G:P, interpreted to be a taphonomic signal (e.g., McCarthy et al., 2003). The G:P ratio was also found to be very high in highstand systems tracts and maximum flooding surfaces where sediment accumulation rates are very low (McCarthy et al., 2003).

Paleobathymetric reconstructions are based on foraminifera, including benthic foraminiferal assemblages, key depth-indicator species, and percentage of planktonic foraminifera (for details, see Katz et al., 2013). Paleodepth constraints use the Miller et al. (1997) general paleobathymetric model, which was established using coeval New Jersey coastal plain sections drilled onshore (as modified by Katz et al., 2013). *Hanzawaia hughesi*–dominated biofacies indicate mid-inner neritic depth (10–25 m), *Pseudononion pizarrensis*–dominated biofacies indicate lower inner neritic to upper middle neritic depth (25–50 m), *Bulimina gracilis*/*Bolivina paula*–dominated biofacies indicate middle-middle neritic depth (50–80 m), and *Uvigerina* spp./*Bolivina floridana*–dominated

TABLE 1. USEFUL DINOCYST DATUMS IN INTEGRATED OCEAN DRILLING PROGRAM EXPEDITION 313 HOLE M0027A

Taxon	LO (sample/depth mcd)	HO (sample/depth mcd)	Range (DN zone)
Trinovantedinium papulum	27A-77R-2/221.11		DN5–
Habibacysta tectata	27A-77R-2/221.11		upper DN5–
Invertocysta lacrymosa	27A-77R-2/221.11		Middle Miocene–
Trinovantedinium harpagonium	27A-80R-1/226.28		DN5–
Unipontedinium aquaeductum	27A-83R-3/237.62	27A-70X-1/207.56	DN5
Imagidinum arachnion	27A-88R-1/250.26		top DN4–DN9
Apteodinium tectatum		27A-70X-1/207.56	–DN5
Cleistosphaeridium placacanthum		27A-73X-1/212.00	–top DN5
Apteodinium spiridoides		27A-88R-2/252.16	–top DN4
Labyrinthodinium truncatum truncatum	27A-88R-1/250.26		base DN4–
Labyrinthodinium truncatum modicum	27A-88R-2/252.16		base DN4–
Cerobrocysta poulsenii	27A-101R-1/290.31		top DN3–DN8
Sumatradinium druggii	27A-102R-2/294.07		base DN3–DN8
Sumatradinium hamulatum	27A-177R-1/503.41	27A- 161R-2/460.51	base DN2–top DN3
Sumatradinium soucouyantiae	27A-186R-1/523.66		base DN2–DN8
Cousteadinium aubryae	27A-186R-1/523.66	27A-83R-3/237.63	DN2–top DN4
Lingulodinium multivirgatum		27A-85R-3/242.72	(–top DN3)
Operculodinium longispinigerum	27A-189R-1/531.08	27A-127R-1/359.71	DN2–DN4
Distatodinium paradoxum		27A-156R-1/445.14	DN2–DN4
Exochosphaeridium insigne	27A-156R-1/445.14	27A-152R-2/434.26	DN2b–DN2c
Cordosphaeridium cantharellus		27A-148R-3/423.66	–DN2b
Cribroperidinium tenuitabulatum		27A-148R-3/423.66	–DN2
Cerebrocysta satchelliae		27A-149R-2/425.56	–DN2
Dinopterigium cladoides		27A-149R-2/425.56	–DN2
Caligodinium amiculum		27A-164R-2/470.46	–DN2a
Membranophoridium aspinatum		27A-176R-1/500.63	–base DN2
Stoverocysta conerae	27A-187R-3/526.08	27A-186R-1/523.66	base DN1–DN2
Chiropterdium galea		27A-186R-1/523.66	–top DN1
Deflandrea phosphoritica		27A-190R-2/525.73	–DN1

Note: LO—lowest occurrence; HO—highest occurrence; DN—dinoflagellate zone; mcd—meters composite depth.

biofacies indicate outer middle neritic depth (>75–100 m). Key taxa (e.g., *Cibicidoides pachyderma*, *Cibicidoides primulus*, *Hanzawaia mantaensis*, *Oridorsalis umbonatus*) often found in high-diversity, low-dominance assemblages indicate outer neritic paleodepths (100–200 m) (for details, see Katz et al., 2013).

Sea level was qualitatively reconstructed, interpreted as high sea level wherever multiple palynological proxies recorded a distal setting and where middle to outer neritic water depths were suggested by the foraminiferal assemblage. These interpretations were at times confounded by barren samples, however, which may indicate either deposition in very shallow water, dissolution, or mass transport of shallow-water sediments into deeper water environments. Sedimentological data proved valuable in verifying our sea-level interpretations, particularly in sediments barren of microfossils and in cases where palynomorphs and foraminifera indicate unrealistic shallow-water environments, likely indicating downslope transport.

Good multiproxy geochronological control is available along the Expedition 313 transect, based on a variety of chronological tools in addition to dinocysts, including Sr isotope age estimates and nannofossil and diatom zonations (Browning et al., 2013). As a result, we were able to assess the influence of changing sea level and climate from the Aquitanian to earliest Serravallian on sedimentation on the New Jersey margin by correlating our sea-level record with Miocene oxygen isotope (Mi) events.

TABLE 2. USEFUL DINOCYST DATUMS IN INTEGRATED OCEAN DRILLING PROGRAM EXPEDITION 313 HOLE M0029A

Taxon	LO (Sample/depth mcd)	HO (Sample/depth mcd)	Range (DN zone)
Ataxodium zevenboomi	29A-64R-1/ 320.96		Serravallian –
Selenopemphix dionaeacysta	29A-70R-1/ 339.13		DN6 –
Trinoventedinium harpagonium	29A-99R-2/425.11		DN5 –
Trinoventedinium papulum	29A-120R-1/470.10		DN5 –
Habibacysta tectata	29A-122R-1/ 481.73		DN5b –
Unipontedinium aquaeductum	29A-128R-3/ 508.79	29A-75R-1/ 353.72	DN5
Cleistosphaeridium placacanthum		29A-85R-2/ 383.25	– top DN5
Cerebrocysta poulsenii	29A-191R-2/ 681.27		top DN3 – DN8
Sumatradinium soucouyantiae	29A-211R-2/ 739.35		base DN2 – DN8
Apteodinium tectatum		29A-101R-1/ 430.84	– DN5
Apteodinium spiridoides		29A-148R-3/ 566.27	– top DN4
Labyrinthodinium truncatum truncatum	29A-176R-1/ 643.82		base DN4 –
Labyrinthodinium truncatum modicum	29A-176R-1/ 643.82		base DN4 –
Sumatradinium druggii	29A-194R-2/690.55		base DN3 – DN8
Cousteaudinium aubryae	29A-212R-1/ 741.04	29A-139R-1/ 536.58	DN2– top DN4
Operculodinium longispinigerum	29A-212R-2/ 742.56	29A-154R-2/ 581.45	DN2– top DN4
Distatodinium paradoxum		29A-148R-3/ 566.27	– top DN4
Exochosphaeridium insigne	29A-204R-1/ 717.71 m	29A-191R-2/ 681.27	DN2b – DN2c
Sumatradinium hamulatum		29A-180R-2/ 657.38	DN2 – top DN3
Cerebrocysta satchelliae		29A-195R-2/ 693.59	–top DN2
Cordosphaeridium cantharellus		29A-196R-2/ 696.93	–DN2b
Stoverocysta conerae	29A-211R-2/ 739.35 m	29A-211R-2/ 739.35	DN1 – DN2
Cribroperidinium tenuitabulatum		29A-212R-1/ 741.04	– top DN2
Dinopterygium cladoides		29A-212R-2/ 742.56	– DN2
Caligodinium amiculum		29A-208R-2/ 730.40	
Membranophoridium aspinatum	29A-217R-1/ 753.87 m	29A-215R-1/ 749.93 m	– base DN2

Note: LO—lowest occurrence; HO—highest occurrence; DN—dinoflagellate zone; mcd—meters composite depth.

PALYNOLOGY OF HOLES 27A AND 29A

Palynological Signature and Age of Miocene Sequences

Each sequence on the New Jersey shallow shelf has a distinct palynological character, not only in assemblages of marine and terrestrial palynomorph species, but in the entire palynofacies present in each slide, including the palynodebris. Sequences identified using seismic and sedimentological criteria have distinct signatures of T:M, Ph:AOM, G:P, and nonsac:bisac pollen, reflecting the distance from the shoreline and sea surface and depositional conditions at each site (Figs. 3–5). Evolution and extinction within dinoflagellate lineages allow biostratigraphic zonation of the uppermost Chattian to lowermost Serravallian, while semiquantitative variations in abundance reflect ecological change (Figs. 6 and 7).

Lithologic Unit VII: Sequence O6

The dinocyst assemblage in sequence O6, above the reflector at 538.68 mcd (meters composite depth) in Hole 27A (Fig. 3), is rich in *Apteodinium tectatum*, *Operculodinium centrocarpum*, *Lingulodinium multivirgatum*, *Spiniferites* spp., *Lejeunecysta* sp., *Brigantedinium* sp., *Membranophoridium aspinatum*, *Cleistosphaeridium placacanthum* and *Dapsilidinium pseudocolligerum* (Supplemental Table 1 [see footnote 1]). The highest occurrence (HO) of *Deflandrea phosphoritica* in sample 27A-190R-2 (147–148 cm, 525.73 mcd) and of *Chiropteridium galea* in sample 27A-186R-1 (95–96 cm, 523.66 mcd), together with *Stoverocysta conerae* in samples 27A-187R-3 (140–141 cm, 526.08 mcd) through 186R-1

TABLE 3. RAW PALYNOMORPH COUNTS FROM INTEGRATED OCEAN DRILLING PROGRAM EXPEDITION 313 HOLE M0027A WITH CALCULATIONS OF THE TERRESTRIAL VERSUS MARINE PALYNOMORPH RATIO AND INTERPRETATIONS OF DEPOSITIONAL ENVIRONMENT AND SYSTEMS TRACTS

Core	Section	Depth in section (cm)	Depth downhole (m)	Terrestrial palynomorphs (grains)	Marine palynomorphs (cysts)	Spike (grains)	T:M	G:P	Environment/ systems tract	Age
63	1	36.0–37.0	189.12	255	27	58	9.44	0.40	OFF	
65	2	24.0–25.0	193.85	175	10	22	17.50	0.50		
66	1	70.0–71.0	195.56	238	30	23	7.93	1.61		
67	2	68.0–70.0	196.01	326.5	18	37	8.82	0.55		
67	2	100.0–102.0	197.37	220	27	25	8.15	0.13		
69	1	40.0–41.0	207.44	217	42	31	5.17	0.15		
70	1	49.0–50.0	207.56	166	63	58	2.63	0.44		
70	2	7.0–8.0	208.5	211	40	12	5.28	0.82		13.2
m4.1			**209**							
71	1	17.0–18.0	209.6	175	50	25	3.50	2.54	SOT	
72	1	14.0–16.0	210.58	94	66	47	1.42	1.20		
72	1	22.0–24.0	210.7	144	103	52	1.39	2.20		
73	1	57.0–58.0	211.45	133	51	7	2.61	1.47		
75	1	50.0–52.0	216.72	137	88	2	1.56	1.15	TST	
75	1	111.0–112.0	217.32	98	77	2	1.27	2.48		
m4.5			**218.39**							
75	2	82.0–83.0	218.53	131	24	6	5.46	2.78	SF	14.8
77	2	40.0–41.0	221.11	155	42	25	3.69	1.41		
m5			**225.45**							
80	1	98.0–99.0	226.28	113	71	9	1.59	3.9	OFF HST MFS	
82	2	24.0–25.0	233.21	89	60	25	1.48	10.8	TST	
m5.2			**236.15**							
83	3	11.0–12.0	237.62	127	52	11	2.44	0.87	SF	15.6
84	2	41.0–42.0	239.47		82.5	78	58	1.06	0.86	
85	3	27.0–28.0	242.72	71	54	28	1.31	1.89	OFF	
88	1	50.0–51.0	250.26	112	51	5	2.19	2.08		
88	2	110.0–111.0	252.86	246	39	6	6.31	12.00	SOT	15.8
m5.3			**256.19**							
91	CC(3)	9.0–10.0	262.05	146	40	12	3.65	1.24	HST	16.8
94	2	100.0–101.0	270.56	320	52	21	6.15	6.14	SF	
94	3	2.0–3.0	271.06		76	40	4	1.90	1.44	TST
m5.3.3			**271.23**						TS	
95	1	109.0–111.0	272.21	170	72	13	2.36	1.83	SOT	
98	1	58.0–60.0	280.08	143	46	11	3.11	2.38	LST	
101	1	90.0–92.0	290.31	171	37	5	4.62	1.12		
101	CC(4)	10.0–11.0	292.8	135	9	3	15.0			
102	2	11.0–13.0	294.07	174	83	74	2.09	2.76		
102	2	47.0–49.0	294.44	228	26	6	8.77	0.73		17.0
m5.4			**295.01**							
103	1	50.0–51.0	296.01	169	89	32	1.89	1.15		17.7
103	1	140.0–141.0	296.91	110	50	22	2.20	2.62		
104	3	36.0–38.0	301.86	173	4	8	43.25			
105	CC(4)	10.0–11.0	304.95	88	26	4	3.38		HST FS	
109	1	110.0–111.0	314.91	229	40	10	5.73	0.67		
114	2	116.0–117.0	331.72	186	57	37	3.26	1.30	FS MFS	
115	1	125.0–126.0	333.36	114	51	28	2.24	1.14	OFF TST	18.0
m5.45			**336.06**							
116	2	38.0–39.0	337.04	175	33	71	5.30	1.29		
122	2	58.0–60.0	347.94	BARREN					channel fill	
m5.47			**355.53**							
126	1	3.0–4.0	358.36	147	14	32	10.50	5.00		
127	1	15.0–16.0	359.71	283	18	38	15.72	2.80	SF	
m5.7			**361.28**							

(*continued*)

(95–96 cm, 523.66 mcd; Fig. 6; Table 1) allow this sequence to be assigned to dinocyst zone DN1 (late Chattian–early Aquitanian, ca. 24.4–22.36 Ma). The existence of the Oligocene-Miocene boundary within this sequence is consistent with the assignment of the lower part of this sequence to nannofossil zone NP25 and the upper part to zone NN1 (Browning et al., 2013).

The AOM-dominated sediments in this sequence (palynofacies type 3 of Batten, 1996; Table 5) are characterized by relatively low terrestrial versus marine palynomorph ratios (mean T:M = 3.11, range 1.24–11.40, n = 11). A strong peak in T:M (11.4) in sample 27A-187R-CC (8–10 cm, 527.68 mcd) is succeeded by somewhat elevated T:M (3.34) in the overlying sample. The abundance of *Homotryblium* spp. in all of the samples above the strong T:M peak (Figs. 3 and 6) suggests equivalence with the Homotryblium spp. zone of Dybkjær and Piasecki (2010) that they correlated with the lower part of the calcareous nannoplankton zone NN2 of Martini (1971), 22.36–21.6(?) Ma. The presence of *Apteodininium spiridoides*, *Hystrichokolpoma rigaudiae*, and *Thalassiphora pelagica* also differentiates the upper part of sequence O6.

Protoperidinioid cysts are not abundant in this sequence (mean G:P = 6.12, range 2.21–10.25, n = 8); *Brigantedinium* spp. is the most consistently present. Most low-diversity pollen assemblages in sequence O6 are dominated by bisaccate conifer pollen (mean nonsac:bisac = 1.00, range 0.5–1.87, n = 5) until the peak in T:M at the base of core 187 (~528 mcd), above which angiosperm pollen become more abundant (mean nonsac:bisac = 2.37, range 1.22–3.56, n = 5; Fig. 3; Table 6). The dominance of gonyaulacoid cysts in marine palynomorph-rich sediments in which the pollen assemblage is characterized by bisaccate grains adapted to long-distance transport is consistent with a distal setting for Site 27 during the early Aquitanian (Fig. 3).

TABLE 3. RAW PALYNOMORPH COUNTS FROM INTEGRATED OCEAN DRILLING PROGRAM EXPEDITION 313 HOLE M0027A WITH CALCULATIONS OF THE TERRESTRIAL VERSUS MARINE PALYNOMORPH RATIO AND INTERPRETATIONS OF DEPOSITIONAL ENVIRONMENT AND SYSTEMS TRACTS (*continued*)

Core	Section	Depth in section (cm)	Depth downhole (m)	Terrestrial palynomorphs (grains)	Marine palynomorphs (cysts)	Spike (grains)	T:M	G:P	Environment/ systems tract	Age
146	CC(3)	8.0–10.0	417.55	115	19	4	6.05			19.2
148	3	10.0–12.0	423.66	124	74	5	1.68	4.83		
149	2	45.0–46.0	425.56	219	46	2	4.76	1.20	river–	
150	2	50.0–51.0	428.66	210	54	8	3.89	1.64	influenced	
151	1	49.0–50.0	430.21	172	32	8	5.38	2.02	SOT	
151	2	145.0–147.0	432.76	141	11	312.82	1.64			
152	2	20.0–21.0	434.26	209	10	6	20.90	2.78		
152	2	104–105	435.10	317.5	34	9	9.34			
154	1	90.0–92.0	440.00	154	32	11	4.81	3.91		
154	CC(3)	0.0–1.0	441.13	223	26	6	8.58			
155	CC(4)	0.0–1.0	445.00	177	84	7	2.11			
156	1	18.0–19.0	445.14	352	58	4	6.07	3.50		
156	2	8.0–10.0	448.09	208	40	3	5.20	3.45		
157	2	122.0–123.0	450.74	123	35	1	3.51	5.80		
159	CC(4)	13.0–15.0	457.54	225	62	6	3.63			
160	2	124.0–126.0	459.88	142	18	7	7.89			
161	2	30.0–31.0	462.01	124	21	5	5.90	0.67		
161	2	89.0–90.0	462.51	227	89	3	2.55	4.20	MFS	
161	CC(4)	8.0–10.0	463.61	172	30	6	5.73			
162	1	89.0–90.0	464.00	121	60	2	2.02	2.29		
162	2	30.0–32.0	464.69	181	91	9	1.99	1.74	TST	
163	1	115.0–116.0	467.46	277	60	12	4.62	0.94		
164	1	110.0–111.0	468.96	226	24	2	9.42	1.00		
164	2	110.0–111.0	470.46	219	36	6	6.44	7.50		
165	1	115.0–116.0	473.16	210	46	12	4.56	2.21		
165	CC(4)	5.0–7.0	475.81	182	27	10	6.74		Toe of	
166	1	15.0–16.0	475.62	136	30	9	4.69	2.63	slope	
169	2	129.0–131.0	487.68	312	95	11	3.28	7.33	apron	
170	1	15.5–16.5	488.17	209	44	13	4.75	0.63		
171	2	120.0–121.0	492.09	178	21	5	8.48	0.75	LST	
171	CC(3)	11.0–13.0	492.46	108	42	5	2.57			
174	1	101–102	494.77	81	59	8	1.37	48.00		20.1
m5.8			**494.87**							
175	1	28.0–29.0	497.09	128	51	14	2.51	0.85		
175	CC(4)	13.0–16.0	500.23	178	37	5	4.81		Toe of	20.4
176	1	77.0–78.0	500.63	120	41	42	2.93	1.73		
177	1	50.0–52.0	503.41	232	40	10	5.80	12.33	slope	
177	CC(4)	14.0–16.0	506.36	165	11	8	15.00		apron	20.6
m6			**509**							
185	CC(2)	15.0–17.0	520.96	111	50	6	2.22	5.60		23.0
186	1	95.0–96.0	522.66	214	67	27	3.19	3.33		
187	1	87–88	523.57	193	129	43	1.49	9.00		
187	3	140–141	526.08	213.5	64	36	3.34	8.33		
187	CC(4)	8.0–10.0	527.68	171	15	5	11.40			
188	2	60.0–61.0	529.21	129	45	17	2.87	2.21	apron	
188	CC(3)	8.0–9.0	530.17	130	82	2	1.59			
189	1	72.0–73.0	531.08	142	51	31	2.78		5.00	
189	CC(4)	6.0–8.0	533.58	198	75	9	2.64			
190	2	119.0–120.0	535.73	110	89	40	1.24		10.25	
190	3	13.0–15.0	536.54	185	128	16	1.45		5.20	
O6			**538.68**							

Note: T:M—terrestrial vs. marine palynomorph ratio; G:P—gonyaulacoid versus protoperidinioidcyst ratio; SF—shoreface (0–10 m); OFF—offshore; SOT—shoreface-offshore transition (10–30 m); TST—transgressive systems tract; FS—flooding surface; LST—lowstand systems tract; HST—highstand systems tract; MFS—maximum flooding surface; TS—transgressive surface.

Lithologic Unit VII: Sequence m6

The boundary between sequences O6 and m6 is characterized by high terrestrial versus marine palynomorph ratio (T:M = 15 in sample 27A-177R-CC, 506.36 mcd), a characteristic signature of erosional unconformities (Figs. 3 and 5; Table 3). The dinocyst assemblage in sequence m6 is relatively rich in *Cleistosphaeridium placacanthum*, *Apteodinium tectatum*, *Dapsilidinium pseudocolligerum*, *Operculodinium longispinigerum*, *Selenopemphix nephroides*, *Lejeunecysta* spp., and *Brigantedinium* spp. (Figs. 6 and 7). In addition to these common cysts, the presence of *Sumatradinium hamulatum* together with *Caligodinium amiculum* (Figs. 6 and 7; Tables 1 and 2) constrains the age of this sequence to DN2a (22.36–19.4 Ma). The HO of *Membranophoridium aspinatum* (27A-176R-1, 500.63 mcd and 29A-215R-1, 749.93 mcd) occurs far below the HO of *Caligodinium amiculum* that marks the subzone DN2a-DN2b boundary. We use this datum to characterize the base of DN2 as older than 20 Ma.

T:M values remain relatively high in this sequence in Hole 27A (mean T:M = 6.21, n = 5), although terrestrial palynomorphs decline somewhat in relative abundance upcore within the thin sequence m6 to T:M = 4.81 in sample 27A-175R-CC (13–16 cm, 500.23 mcd) from a peak value of 15 just above the sequence boundary. Lower T:M values were measured in the three samples analyzed from this thin sequence in the more distal Hole 29A (mean T:M = 3.04, range 1.20–4.26). Angiosperm pollen outnumber bisaccate conifer pollen in this sequence at both sites (Figs. 3 and 4; Table 6). This taphonomic signature records increased terrigenous flux to the New Jersey margin during the Aquitanian.

No other microfossil groups were biostratigraphically useful, but Sr ages of 20.7–19.0 at the top of this sequence are consistent with the dinocyst zonation (Browning et al., 2013).

TABLE 4. RAW PALYNOMORPH COUNTS FROM INTEGRATED OCEAN DRILLING PROGRAM EXPEDITION 313 HOLE M0029A WITH CALCULATIONS OF THE T:M PALYOMORPH RATIO AND INTERPRETATIONS OF DEPOSITIONAL ENVIRONMENT AND SYSTEMS TRACT

Core	Section	Depth in section (cm)	Depth downhole (m)	Terrestrial palynomorphs (grains)	Marine palynomorphs (cysts)	Spike (grains)	T:M	G:P	Environment or systems tract (Miller et al., 2013a)	Age (Ma) (Browning et al., 2013)
51	1	115.0–116.0	284.31	131	20	35	6.55			
53	1	91.0–92.0	293.11	149	30	24	4.97			
62	1	116.0–117.0	314.81	163	53	16	3.07	0.92		
63	2	14.0–15.0	318.11	157	51	16	2.20	1.75		
64	1	120.0–121.0	320.96	572	146	38	3.92	1.71		
65	2	18.0–19.0	324.50	174	17	33	10.24		SF	
66	1	25.0–26.0	326.11	162	24	8	6.75	0.25		
69	1	44.5–46.0	335.46	620	129	38	4.81	0.35		
70	1	107.0–108.0	339.13	186	42	17	4.43	2.88	OFF	12.9
m4.1			**342.81**							
72	2	39.0–40.0	345.20	168	25	17	6.72		SB	12.9
73	CC			219	60	25	3.65	3.5		
74	2	57.0–58.0	352.32	246	77	11	3.19	1.69	FS	
75	1	41.0–42.0	353.72	98	40	3	2.45	0.79		13.0
77	1	119.0–120.0	357.55	366	161	51	2.27	3.52	LST	13.0
78	1	110.0–111.0	360.51	143	32	5	4.47	3.11		
m4.2			**364.86**							
80	1	109.0–110.0	366.60	194	79	6	2.45	1.00		
83	1	10.0–11.0	374.76	284	83	11	3.42	0.46		13.1
m4.3			**377.15**							
84	2	122.0–123.0	380.48	139	68	6	2.04	1.56		13.1
85	2	99.0–100.0	383.25	312	123	8	2.54	3.86		
85	CC		385.75	211	84	9	2.52	1.47		
88	1	102.0–103.0	390.93	296	123	14	2.41	1.56		
90	2	81.0–82.0	398.31	98	66	9	1.48	1.44		
92	1	100.0–101.0	403.11	115.5	89	5	1.30	1.87		
93	2	123.0–124.0	407.72	146	35	6	4.17			13.2
m4.4			**408.65**							
94	2	110.0–111.0	410.81	184	56	7	3.34	1.67		13.2
95	1	41.0–42.0	411.67	111	65	6	1.71	2.61	OFF	
98	2	70.0–71.0	421.26	179	29	4	6.17			
99	2	14.0–15.0	425.11	159	22	2	7.23	0.89		
101	1	128.0–129.0	430.84	393	54	11	7.28	0.75	HST	
104	1	98.0–99.0	439.69	183	17	2	10.76	1.54		
106	2	36.0–37.0	443.62	211	27	5	5.31	0.44		
107	3	40.0–41.0	447.81	83	59	6	1.41	2.67	MFS	
109	2	20.0–21.0	452.61	269	43	7	6.26	13.00		
110	2	21.0–22.0	455.39	204	43	12	4.74			
111	1	92.0–93.0	457.93	268	24	5	11.17	7.17		
113	1	102.0–103.0	464.13	254	77	22	3.30	2.15		
114	1	35.0–37.0	466.51	123	37	12	3.32	3.11		
116	1	120.0–121.0	473.46	59	106	14	0.56	3.04	TS	13.6
m4.5			**478.61**							
120	1	32.0–33.0	481.73	105	30	5	3.50	3.00		13.6
121	2	113.0–114.0	487.10	103	34	6	3.03	4.50	apron	
122	1	150.0–151.0	489.01	136	49	5	2.78	0.50	lobe	
126	1	15.0–16.0	499.86	196	86	11	2.28	1.54		13.7
m5			**502.01**							
127	3	31.0–32.0	505.35	168	58	3	2.90			14.6
128	3	73.0–74.0	508.79	105	82	12	1.28	2.35		
129	1	89.0–90.0	509.75	162	68	2	2.38			
130	2	32.0–33.0	513.73	122	56	7	2.18	1.56		
131	1	28.0–29.0	515.24	118	70	6	1.69	1.09		
132	2	30.0–31.0	519.81	127	50	2	2.54			
133	1	48.0–49.0	521.54	137	55	6	2.49	2.6		
136	1	73.0–74.0	528.48	321	89	19	3.61	0.74		
137	1	90.0–91.0	531.11	212	64	8	3.31	0.63	HST	
138	2	49.0–50.0	535.27	85	59	15	1.44	1.81		
139	1	27.0–28.0	536.58	115	56	6	2.05	2.73		
140	2	119.0–120.0	541.1	151	70	8	2.16			
141	1	84.0–85.0	543.25	162	36	7	4.50			
142	2	76.0–77.0	547.72	307	110	12	2.79	2.71		
143	1	33.0–34.0	548.84	142	24	1	5.92			
144	1	29.0–30.0	551.85	102	43	15	2.37	2.10		
146	1	8.0–9.0	555.14	118	38	2	3.11			
147	1	14.0–15.0	557.8	114	31	1	3.68			
148	3	30.0–31.0	563.25	188	44	9	4.27	3.44		

(*continued*)

TABLE 4. RAW PALYNOMORPH COUNTS FROM INTEGRATED OCEAN DRILLING PROGRAM EXPEDITION 313 HOLE M0029A WITH CALCULATIONS OF THE T:M PALYOMORPH RATIO AND INTERPRETATIONS OF DEPOSITIONAL ENVIRONMENT AND SYSTEMS TRACT (*continued*)

Core	Section	Depth in section (cm)	Depth downhole (m)	Terrestrial palynomorphs (grains)	Marine palynomorphs (cysts)	Spike (grains)	T:M	G:P	Environment or systems tract (Miller et al., 2013a)	Age (Ma) (Browning et al., 2013)
149	3	10.0–11.0	566.27	106	36	8	2.94	3.00		
151	3	17.0–18.0	572.43	174	31	5	5.61	0.83		
152	2	27.0–28.0	574.68	164	28	5	5.86			
153	2	50.0–51.0	577.99	133	43	1	3.09			
154	2	90.0–91.0	581.45	102	35	13	2.91	2.89		
155	2	99.0–100.0	584.55	104	54	3	1.93			
156	1	20.0–21.0	585.31	135	64	3	2.04	1.17	TST	
158	2	5.0–6.0	591.96	222	45	16	4.93	1.93		
160	1	28.0–29.0	597.59	140	47	4	2.98	3.60		
161	2	33.0–34.0	602.21	132.5	47	5	2.82			15.6
m5.2			**602.25**							
163	1	73.0–74.0	607.19	296	37	4	8.00	1.42		15.8
165	2	154.0–156.0	615.64	132	84	10	1.57	6.27		
167	2	151.0–153.0	621.68	107	31	3	3.45	0.82		
168	1	21.0–22.0	621.92	131	47	5	2.79		toe-of-slope	
168	2	96.0–97.0	624.17	102	55	31	1.85	3.78	apron	
170	2	150.0–152.0	630.82	136	49	15	2.78	15.33		
173	1	154.0–156.0	636.76	117	67	10	1.75	8.14		
175	2	110.0–111.0	642.62	283	130	9	2.18	2.39		16.1
m5.3			**643.19**							
176	1	76.0–77.0	643.82	119	45	7	2.64	3.89	OFF	17.6
179	2	5.0–6.0	650.99	345	100	6	3.45	2.00		
180	1	38.0–39.0	652.59	166	39	7	4.26	4.51	Toe of slope apron	
181	2	62.0–63.0	657.38	108	33	4	3.27	1.23		
182	2	38.0–39.0	660.13	103	63	8	1.63			
182	2	99.0–100.0	660.81	268	21	8	12.76			17.7
m5.4			**662.37**							
183	1	110.0–111.0	663.81	249	91	21	2.74	3.17		17.7
184	1	113.0–114.0	665.54	158	49	11	3.22	2.77	Toe of slope apron	
185	1	9.0–10.0	666.85	141	20	4	7.05			
187	2	27.0–28.0	672.25	148	23	23	6.43			17.8
m5.45			**673.71**							
189	CC		675.5	242	47	8	5.15			17.9
190	1	130.0 -131.0	677.84	94	51	12	1.84	1.32		
190	2	34.0–35.0	678.45	222	147	13	1.59	1.73		
191	2	22.0–23.0	681.27	254	121	12	2.10	1.71		
192	1	88.0–89.0	683.59	97	30	8	3.23	1.78		
192	2	98.0–99.0	685.2	196	67	5	2.93			18.0
194	2	23.0–24.0	690.55	241	86	11	2.80	2.31		18.1
195	1	50.0–51.0	692.36	178	57	5	3.12			
195	2	33.0–35.0	693.59	198	93	28	2.13	8.33		
195	2	124.0–125.0	694.60	128.5	49	1	2.62	4.88		
m5.47			**696**							
196	2	50.0–52.0	696.93	248	96	16	2.58	3.92		
197	2	119.0–120.0	700.65	162	37	9	4.38			
199	2	46.0–47.0	706.02	218	127	12	1.72	6.89		18.3
m5.6			**706.66–710**							
201	1	6.0–7.0	710.22	147	43	3	3.42			18.6
202	1	9.0–10.0	711.87	152	39	4	3.90			
202	2	6.0–7.0	712.96	113	52	2	2.17	2.07		
203	1	22.0–23.0	713.43	142	70	2	2.03	2.67		
204	1	145.0–147.0	717.71	202	126	16	1.60	7.89	OFF	
205	CC		723.10	170	41	7	4.15			18.8
207	3	28.0–30.0	728.51	193	44	16	4.39			20.0
m5.7			**728.56**							
208	2	44.0–45.0	730.40	126	52	25	2.42	1.83		
209	1	111.0–112.0	732.62	152	65	59	2.34	1.56		
210	2	30.0–31.0	736.36	158	47	20	3.36		dysoxic	
211	1	31.0–32.0	737.92	130	11	26	11.82	4.50	prodelta	
211	2	24.0–25.0	739.35	113	98	82	1.15	2.27		
212	1	38.0–39.0	741.04	105	22	42	4.77	1.92		
212	2	84.0–85.0	742.56	169	112	30	1.51	2.86		20.2
m5.8			**746**							
215	2	5.0–6.0	749.93	95	79		1.20	2.76		20.5
217	1	101.0–102.0	753.87	216	29	4	3.67	3.92		
217	2	103.0–104.0	755.35	145	34	6	4.26			

Note: T:M—terrestrial vs. marine palynomorph ratio; G:P—gonyaulacoid versus protoperidinioid cyst ratio; SF—shoreface (0–10 mP; OFF—offshore (>30 m); SB—sequence boundary; FS—flooding surface; LST—lowstand systems tract; HST—highstand systems tract; MFS—maximum flooding surface; TS—transgressive surface.

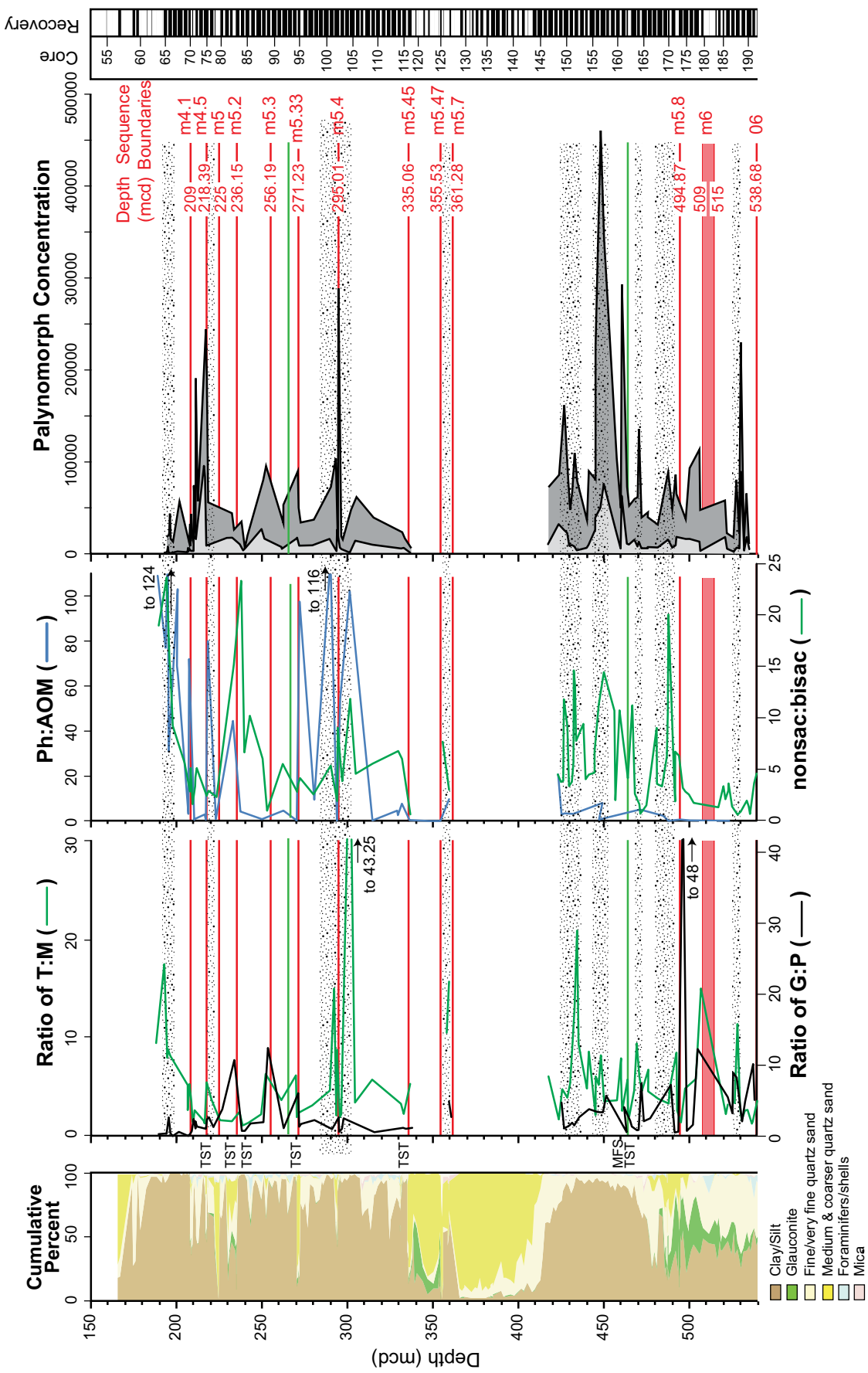

Figure 3. Ratio of terrestrial versus marine palynomorphs (T:M—green line), gonyaulacoid versus protoperidinioid dinocysts (G:P—black line), phytoclast versus amorphous organic matter (Ph:AOM—blue line), and nonsaccate versus bisaccate conifer pollen (nonsac:bisac—green line) and absolute abundance (concentration/cm^3) of palynomorphs: marine dinocysts + acritarchs, (pale gray) and terrigenous pollen + embryophyte spores (dark gray) in Integrated Ocean Drilling Program Hole 27A. Stipple highlights coeval peaks in T:M, Ph:AOM, and nonsac:bisac that record increased terrigenous flux to Site 27. These are generally associated with peaks in total palynomorph abundance (concentration) and very low G:P, recording rapid burial inhibiting oxidation of susceptible protoperidinioid cysts. In contrast, transgressive systems tracts (TST) and maximum flooding surfaces (MFS) (from Miller et al., 2013a) are characterized by high G:P and low T:M, Ph:AOM, and nonsac:bisac. Seismic reflectors O6 to m4.1 (red lines) are sequence boundaries (i.e., impedance contrasts) identified during Expedition 313 and subsequently adjusted (Mountain et al., 2010; Miller et al., 2013a). Depth—meters composite depth (mcd).

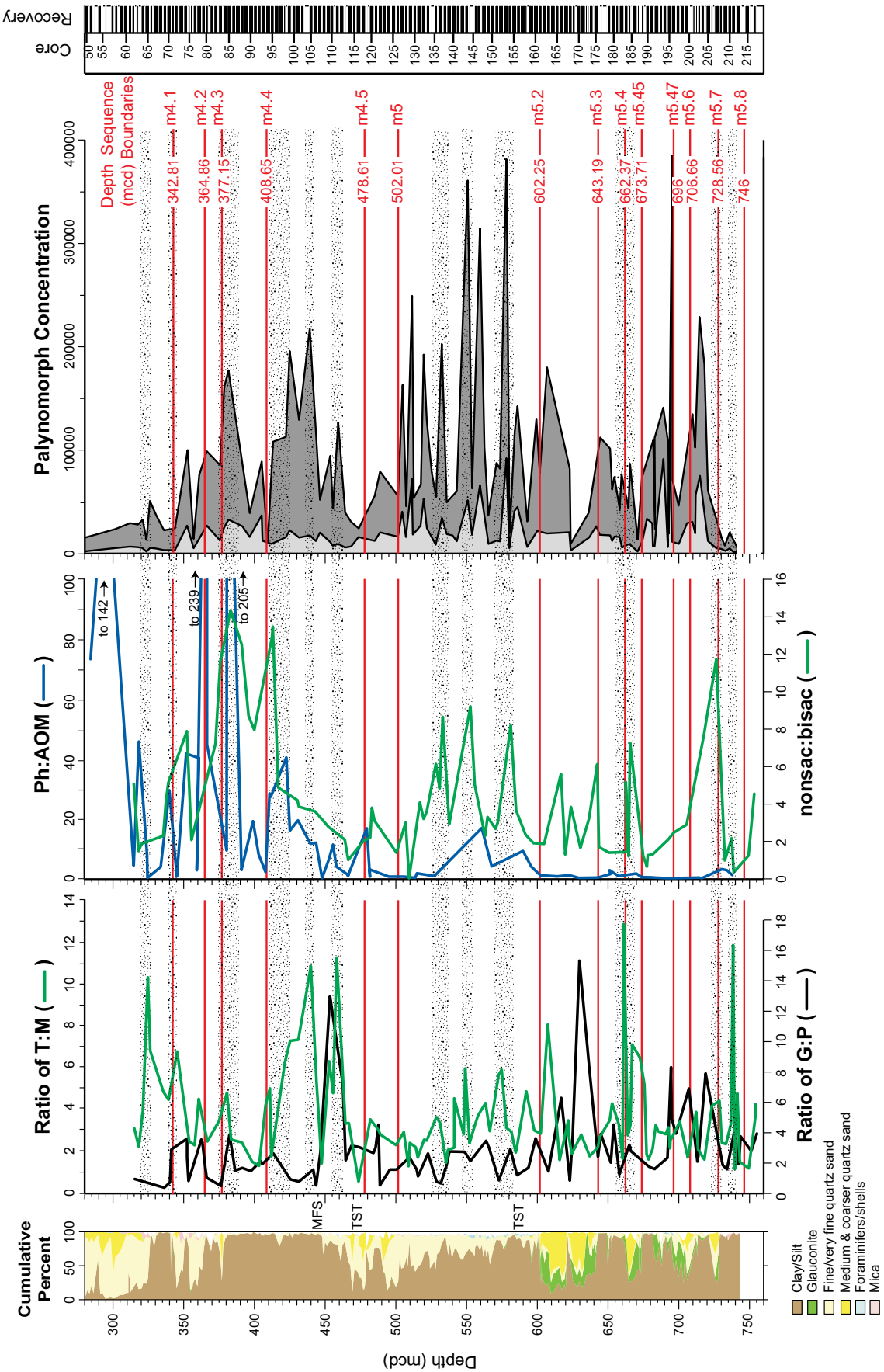

Figure 4. Ratio of terrestrial versus marine palynomorphs (T:M—green line), gonyaulacoid versus protoperidinioid dinocysts (G:P—black line), phytoclast versus amorphous organic matter (Ph:AOM—blue line) and nonsaccate versus bisaccate conifer pollen (nonsac:bisac—green line) and absolute abundance (concentration per cm^3) of palynomorphs (marine: dinocysts + acritarchs, pale gray) and terrigenous (pollen + embryophyte spores, dark gray) in Hole 29A. Depth—meters composite depth (mcd). Stipple highlights coeval peaks in T:M, Ph:AOM, and nonsac:bisac that record increased terrigenous flux to Site 29. These are generally associated with peaks in total palynomorph abundance (concentration) and very low G:P, recording rapid burial inhibiting oxidation of susceptible protoperidinioid cysts. Transgressive systems tracts (TST) and maximum flooding surfaces (MFS) (from Miller et al., 2013a) are characterized by high G:P and low T:M, Ph:AOM, and nonsac:bisac. Seismic reflectors m5.8 to m4.1 (red lines) are sequence boundaries (i.e., impedance contrasts) identified during Integrated Ocean Drilling Program Expedition 313 and subsequently adjusted (Mountain et al., 2010; Miller et al., 2013a).

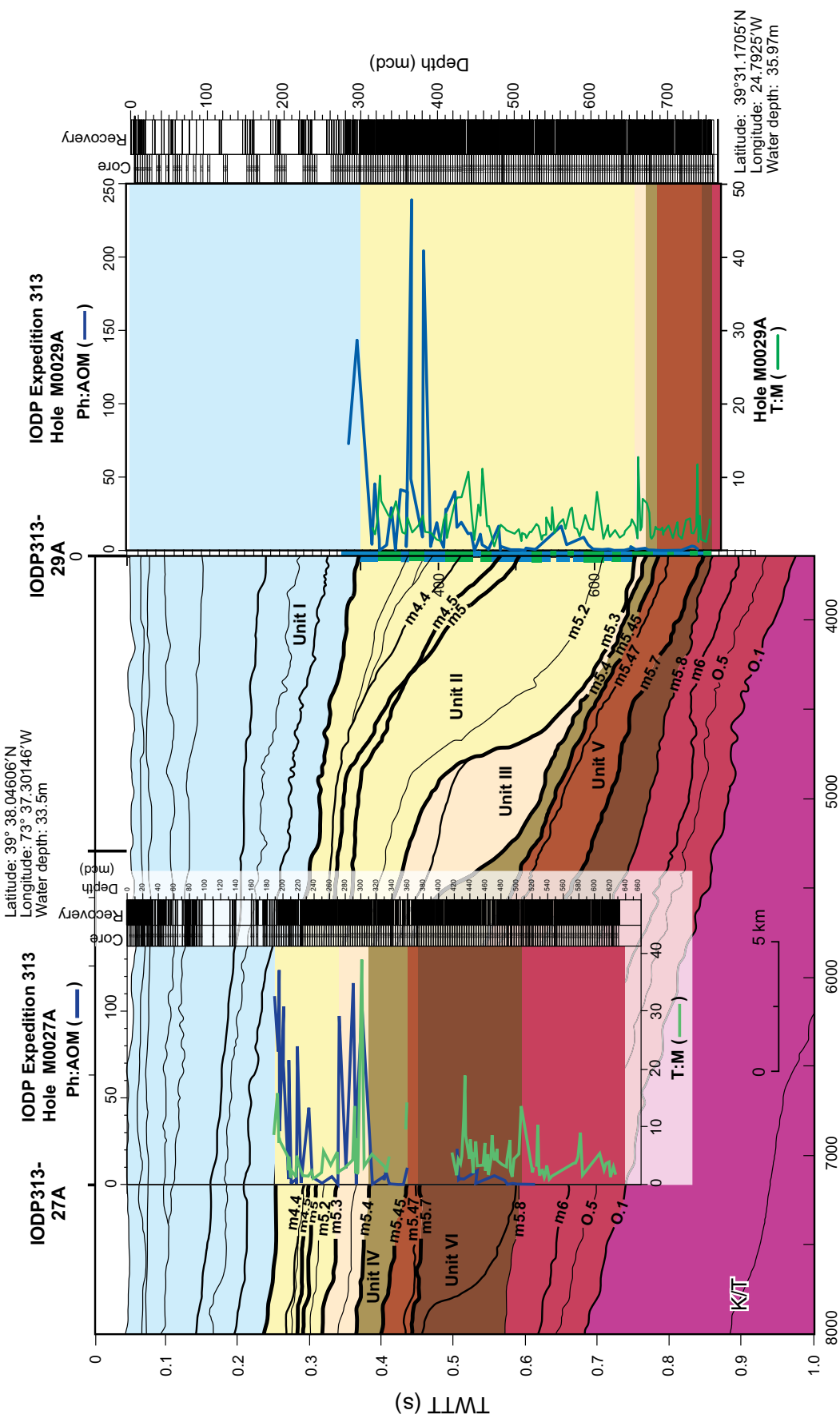

Figure 5. The palynofacies (i.e., the acid-resistant organic fraction of the sediment) clearly characterizes the lithological units and unconformity bounded sequences in Integrated Ocean Drilling Program (IODP) Holes 27A and 29A. Terrigenous flux, represented by high T:M (terrestrial versus marine palynomorphs—green curve) and high Ph:AOM (phytoclast versus amorphous organic matter—blue curve), is especially high in lithologic unit III around sequence boundary m5.4 (where the highest T:M peak was measured in both holes) and in upper lithologic unit II around sequence boundaries m4.5, m4.3, m4.2, and m4.1. Ph:AOM increases dramatically when the shelf progrades past each site, whereas peaks in T:M appear to be generated by increased proximity to the shoreline and accelerated resedimentation of terrigenous particles seaward, particularly past the shelf break. K/T is Cretaceous-Tertiary (Paleogene) boundary.

TABLE 5. PHYTOCLAST VERSUS AMORPHOUS ORGANIC MATTER AND PALYNOFACIES TYPE IN INTEGRATED OCEAN DRILLING PROGRAM EXPEDITION 313 HOLES M0027A AND M0029A

Hole	Core	Section	Depth in core	Depth mcd	Phytoclasts	AOM	Ph:AOM	Palynofacies type
27A	63	1	36.0–37.0	189.12	109	1	109	1
27A	65	2	24.0–25.0	193.85	154	2	77	1
27A	65	CC	195.22	124	1	124	1	
27A	66	1	70.0–71. 0	195.56	93	3	31	1
27A	67	2	68.0–70.0	196.01	103	1	103	1
27A	67	2	100.0–102.0	197.37	69	1	69	1
27A	67	CC	201.05	65	1	65	1	
27A	69	CC	207.10	86	26	3.31	1	
27A	70	1	49.0–50.0	207.56	72	1	72	1
m4.1				**209.00**				
27A	72	1	14.0–16.0	210.58	38	54	0.70	2
27A	72	1	22.0–24.0	210.70	46	50	0.92	2
27A	75	1	50.0–52.0	216.72	67	22	3.05	1
27A	75	1	111.0–112.0	217.32	38	58	0.66	2
m4.5				**218.39**				
27A	75	2	82.0–83.0	218.53	80	1	80.00	1
27A	77	1	90.0–91.0	223.21	37	37	1.00	2
m5				**225.45**				
27A	82	2	24.0–25.0	233.21	89	2	44.50	1
m5.2				**236.15**				
27A	83	3	11.0–12.0	237.62	161	37	4.35	1
27A	88	1	50.0–51.0	250.26	120	126	0.95	2
m5.3				**256.19**				
27A	91	CC	262.05	197	42	4.69	1	
27A	94	2	100.0–101.0	270.56	65	164	0.40	2
m5.3.3				**271.23**				
27A	95	1	109.0–111.0	272.21	195	2	97.50	1
27A	98	1	58.0–60.0	280.08	192	20	9.60	1
27A	101	1	90.0–92.0	290.31	233	2	116.50	1
27A	102	2	11.0–13.0	294.07	42	168	0.25	2
m5.4				**295.01**				
27A	103	1	50.0–51.0	296.01	54	1	54.00	1
27A	105	CC	304.95	102		102.00	1	
27A	109	1	110.0–111.0	314.91	20	54	0.37	2
27A	114	1	33–34	329.39	176	37	4.76	1
27A	114	1	71–73	329.77	145	53	2.74	1
27A	115	1	125.0–126.0	333.36	180	23	7.83	1
m5.45				**336.06**				
27A	116	2	38.0–39.0	337.04	69	135	0.51	2
27A	122	2	58.0–60.0	347.94	10	85	0.11	2
27A	125	1	47–48	354.59	23	167	0.14	2
m5.47				**355.53**				
27A	127	1	15.0–16.0	359.71	226	23	9.83	1
m5.7				**361.28**				
27A	148	3	10.0–12.0	423.66	208	10	20.80	1
27A	149	2	45.0–46.0	425.56	144	50	2.88	1
27A	150	1	55–56	427.21	178	51	3.49	1
27A	151	2	110.0–111.0	432.31	163	50	3.26	1
27A	157	2	122.0–123.0	450.74	178	22	8.09	1
27A	163	1	115.0–116.0	467.46	98	128	0.77	2
27A	164	2	110.0–111.0	470.46	176	34	5.18	2
27A	169	1	484.93	143		58	2.47	3
27A	170	1	15.5–16.5	488.17	36	187	0.19	2
27A	174	1	101–102	494.77	88	11	0.80	2
m5.8				**494.87**				
27A	176	1	77.0–78.0	500.63	63	156	0.40	2
m6				**509**				
27A	186	1	95.0 –96.0	522.66	39	164	0.24	3
O6				**538.68**				
29A	51	1	115–116	284.31	220	3	73.33	1
29A	54	CC		294.71	142	1	142.00	1
29A	62	1	116–117	314.81	154	36	4.28	1
29A	63	2	14–15	318.11	183	4	45.75	1
29A	64	CC	324.30	191	25	7.64	1	
29A	65	2	18–19	324.49	19	176	0.11	2
29A	67	CC	333.94	115	30	3.83	1	
29A	69	CC	339.99	147	5	29.40	1	
m4.1				**342.81**				
29A	72	2	39–40	345.21	83	134	0.62	2
29A	73	CC	351.8	125	3	41.67	1	

(*continued*)

TABLE 5. PHYTOCLAST VERSUS AMORPHOUS ORGANIC MATTER AND PALYNOFACIES TYPE IN INTEGRATED OCEAN DRILLING PROGRAM EXPEDITION 313 HOLES M0027A AND M0029A (*continued*)

Hole	Core	Section	Depth in core	Depth mcd	Phytoclasts	AOM	Ph:AOM	Palynofacies type
29A	77	CC	359.41	161	4	40.25	1	
29A	78	CC	360.82	143	53	2.70	2	
m4.2				**364.86**				
29A	80	1	109–110	366.60	239	1	239.00	1
29A	81	1	109–111	368.10	224	5	44.80	1
m4.3				**377.15**				
29A	84	2	122–123	380.43	195	21	9.29	1
29A	85	CC	385.75	205	1	205.00	1	
29A	88	1	102–103	390.93	146	52	2.81	2
29A	91	CC	399.06	210	11	19.09	1	
29A	92	1	100–101	403.11	184	23	8.00	1
29A	93	2	123–124	407.72	133	62	2.15	2
m4.4				**408.65**				
29A	94	2	110–111.	410.81	199	7	28.43	1
29A	95	1	41–42	411.67	218	8	27.25	1
29A	98	2	70–71	421.26	202	5	40.40	1
29A	99	2	14–15	425.11	223	14	15.93	1
29A	101	1	128–129	430.84	233	12	19.42	1
29A	104	1	98–99	439.69	196	17	11.53	1
29A	106	2	36–37	443.62	191	16	11.94	1
29A	107	3	40–41	447.81	7	224	0.03	2
29A	109	2	20–21	452.61	156	25	6.24	1
29A	110	2	21–22	455.39	180	16	11.25	1
29A	111	1	92–93	457.93	176	45	3.91	1
29A	114	1	35–37	466.51	103	93	1.11	2
29A	114	CC	467.16	94	132	0.71	2	
m4.5				**478.61**				
29A	119	CC	479.50	184	11	16.73	1	
29A	120	1	32–33	481.73	66	126	0.53	2
29A	124	2	32–33	495.11	74	127	0.58	2
m5				**502.01**				
29A	127	3	31–32	505.35	76	127	0.60	2
29A	130	2	32–33	513.73	24	159	0.15	3
29A	131	CC	514.96	136	80	1.70	2	
29A	135	CC	527.16	80	103	0.78	2	
29A	148	CC	560.71	185	11	16.82	1	
29A	150	1	95–96	567.76	168	42	4.00	1
29A	157	2	20–21	589.86	192	21	9.14	1
29A	159	2	20–21	595.76	150	38	3.94	1
29A	161	2	33–34	602.21	105	110	0.95	2
m5.2				**602.25**				
29A	165	2	154–156	615.64	82	133	0.62	2
29A	168	1	21–22	621.92	125	128	0.98	2
29A	168	2	96–97	624.17	75	92	0.82	2
29A	170	2	150–152	630.82	34	198	0.17	3
29A	175	2	110–111	642.62	37	187	0.20	2
m5.3				**643.19**				
29A	178	2	67–68	649.62	130	93	1.40	2
29A	179	2	5–6	650.99	173	63	2.75	2
29A	181	2	62–63	657.38	55	75	0.73	2
m5.4				**662.37**				
29A	186	2	95–96	669.91	121	77	1.57	2
29A	188	2	60–61	673.81	59	145	0.41	2
m5.45				**673.71**				
29A	191	2	22–23	681.27	49	180	0.27	2
29A	192	1	88–89	683.59	31	166	0.19	3
29A	194	2	23–24	690.55	14	238	0.06	3
29A	195	2	124–125	694.60	8	196	0.04	3
m5.47				**696**				
29A	196	2	50–52	696.93	15	205	0.07	3
m5.6				**706.66–710**				
29A	202	2	6–7	712.96	37	184	0.20	2
29A	204	1	145 –147	717.71	9	195	0.05	3
m5.7				**728.56**				
29A	208	2	44–45	730.40	142	47	3.02	1
29A	209	1	111–112	732.62	143	53	2.70	1
29A	210	2	30–31	736.36	74	66	1.12	2
m5.8				**746**				

Note: Ph—Phytoclast (Ph); AOM—amorphous organic matter; MCD—meters composite depth.
*Palynofacies type following Batten (1996).

TABLE 6. RATIOS OF NONSACCATE VERSUS BISACCATE POLLEN FROM INTEGRATED OCEAN DRILLING PROGRAM EXPEDITION 313 HOLES M0027A AND M0029A AND SUMMARY OF POLLEN DATA FROM HOLE M0027A

Hole	Core	Section	Depth in core	Depth mcd	Nonsac:Bisac	Bisac	TCT	Hemlock	Oak	Hickory	Elm	Palm	Other	Total
27A	65R/	2	24–25	193.85	23.71	10.5	8	0	152	10	6	2	71	259.5
27A	66R	1	70–71	195.60	17.27	11	13	0	66	11	2	0	98	201
27A	67R	2	68–70	196.01	14.41	17	14	2	134	27	2	0	66	262
27A	67R	2	100–101	199.10	17.00	15	16	2	94	16	9	0	118	270
27A	69R	1	40–41	204.41	5.56	52.5	8	0	126	32	6	0	120	344.5
27A	70R	1	49–50	207.60	6.30	37	20	0	126	17	5	0	64	270
27A	70R	2	7–8	208.70	10.20	24.5	19	0	182	8	3	0	38	274.5
m4.1				**209**										
27A	71R	1	17–18	209.10	2.64	88	18	0	151	10	6	0	47	320
27A	72R	1	22–24	210.70	4.18	50.5	17	0	132	15	2	0	45	261.5
27A	73R	1	57–58	211.45	5.06	50	18	0	150	14	6	0	65	303
m4.5				**218.39**										
27A	75R	2	82–83	218.53	2.85	87.5	16	1	150	17	7	0	58	336.5
27A	77R	1	90–91	223.21	2.22	95	16	0	132	3	5	5	50	306
m5				**225.45**										
27A	80R	1	92–93	226.48	6.41	39	11	0	162	18	5	0	54	289
27A	82R	2	24–25	233.21	15.20	15	37	1	134	12	1	1	42	243
m5.2	x	x	x	**236.15**										
27A	83R	3	11–12	239.21	23.40	10	10	0	169	8	9	0	38	244
27A	84R	2	41–42	238.6	18.72	12.5	13	0	157	11	0	0	53	246.5
27A	85R	3	27–28	242.72	10.18	22.5	8	0	172	13	4	0	32	251.5
27A	88R	1	50–51	250.26	5.98	42.5	29	0	167	5	5	0	48	296.5
m5.3				**256.19**										
27A	91R	CC	9–10	262.05	5.46	41	2	0	135	29	7	0	51	265
27A	95R	1	109–111	272.21	4.08	62	18	0	123	29	8	0	75	315
27A	101R	1	90–92	290.31	5.31	49	18	0	144	21	6	6	65	309
27A	104R	CC	x	301.61	11.84	19	4	0	113	32	9	1	66	244
27A	105R	CC	0–11	304.95	4.51	47.5	6	0	85	65	5	0	53	261.5
27A	109R	1	10–11	314.91	5.45	45.5	17	0	151	3	3	0	76	295.5
27A	114R	1	71–73	329.77	6.73	20.5	11	0	65	18	2	2	40	158.5
27A	115R	1	3–4	332.14	5.96	24	13	0	53	15	3	6	53	167
m5.47				**355.53**										
27A	127R	1	15–16	359.71	2.94	78	22	2	122	27	2	0	54	307
27A	148R	3	10–12	423.66	4.44	58.5	33	0	152	21	2	0	52	318.5
27A	149R	CC	11–12	426.71	3.81	62.5	10	1	142	15	3	0	67	300.5
27A	150R	1	55–56	427.21	11.80	20	13	1	156	7	4	0	55	256
27A	150R	2	100–101	429.16	9.14	28	24	0	183	5	1	0	43	284
27A	151R	2	55–56.5	431.86	3.71	61	9	0	133	20	2	0	62	287
27A	151R	CC	x	432.86	5.65	40.5	12	0	136	23	2	0	56	269.5
27A	152R	1	20– 21	432.96	14.63	16	7	0	173	12	1	0	42	250
27A	152R	1	99–100	433.75	13.11	18	13	0	179	6	3	0	35	254
27A	153R	2	127–128	438.58	9.38	26	6	0	174	5	2	0	57	270
27A	154R	CC	x	441.91	4.43	54	8	0	151	15	3	0	62	293
27A	155R	CC	x	445.07	4.61	51	19	1	111	26	5	0	73	286
27A	156R	1	18– 19	445.14	6.68	37	16	0	174	7	1	6	43	284
27A	156R	2	114–115	447.60	11.27	20.5	18	0	149	7	2	6	49	251.5
27A	157R	2	122–123	450.74	14.76	17.5	14	0	179	7	1	0	52	270.5
27A	159R	2	120–121	456.82	10.68	23.5	10	0	172	4	2	5	58	274.5
27A	160R	2	32–34	458.96	7.41	32	21	0	143	18	0	3	52	269
27A	160R	CC	x	459.88	10.71	21	13	0	138	25	1	0	48	246
27A	161R	2	30–31	462.01	7.83	30	9	0	145	22	1	0	58	265
27A	162R	2	30–32	464.69	4.08	62	11	2	130	34	6	0	70	315

(*continued*)

TABLE 6. RATIOS OF NONSACCATE VERSUS BISACCATE POLLEN FROM INTEGRATED OCEAN DRILLING PROGRAM EXPEDITION 313 HOLES M0027A AND M0029A AND SUMMARY OF POLLEN DATA FROM HOLE M0027A (*continued*)

Hole	Core	Section	Depth in core	Depth mcd	Nonsac:Bisac	Bisac	TCT	Hemlock	Oak	Hickory	Elm	Palm	Other	Total
27A	163R	1	115–116	467.46	11.21	21.5	11	0	164	13	2	4	47	262.5
27A	164R	2	61–62	471.47	1.53	166.5	20	1	107	45	2	0	79	420.5
27A	166R	1	15–16	475.62	1.41	199	27	10	131	29	1	7	76	480
27A	167R	CC	x	481.60	9.00	24	12	0	109	24	2	0	69	240
27A	168R	1	21–22	481.76	3.52	66	7	0	129	17	11	1	67	298
27A	169R	1	32–33	484.93	3.27	73.5	17	1	146	15	3	1	57	313.5
27A	170R	1	51–52	488.17	20.09	11.5	10	0	173	8	0	0	40	242.5
27A	171R	CC	x	492.47	1.81	129.5	36	4	112	21	3	0	58	363.5
27A	172R	1	14.5–15.5	492.59	6.67	37.5	20	0	170	9	2	0	49	287.5
27A	174R	1	101–103	494.77	6.27	40.5	19	0	171	17	0	0	47	294.5
27A	175R	1	28–29	497.09	3.12	82	38	2	140	11	1	3	61	338
m5.8				**494.87**										
27A	176R	1	77–78	500.63	2.48	92.5	19	0	150	24	2	0	34	321.5
27A	177R	1	50–52	503.41	1.65	142	8	0	171	9	5	0	42	377
m6				**509**										
27A	186R	2	95–96	523.66	2.84	96.5	28	2	172	20	3	1	48	370.5
27A	188R	2	60–61	529.21	0.50	549.5	53	13	117	37	5	2	49	825.5
27A	190R	1	119–120	534.60	1.88	128.5	23	0	129	34	1	0	54	369.5
O6				**538.68**										
29A	62	1	116–117	314.81	5.07	44	3	0	148	22	7	0	44	268
29A	63	2	14–15	318.11	1.48									
29A	64	1	120–121	320.21	1.87	126.5	41	6	92	20	7	0	60	352.5
29A	69	1	44.5–55.5	335.46	2.29	96.5	14	0	80	40	8	0	77	315.5
29A	69	2	103–105	337.55	4.21	53	36	2	89	15	9	0	74	278
29A	70	1	107–108	339.13	5.13									
m4.1				**342.81**										
29A	74	2	57–58	352.32	7.88									
29A	76	1	120–121	355.55	2.08	108	24	0	130	18	4	1	41	326
m4.2				**364.86**										
29A	82	1	93–94	372.54	7.20	30.5	16	0	101	21	3	1	74	246.5
29A	83	1	10–11	376.00	11.60									
m4.3				**377.15**										
29A	85	2	99–100	383.10	14.33	15	15	0	125	21	7	1	50	234
29A	88	1	102–103	390.93	12.50									
29A	90	2	81–82	396.00	8.70									
29A	92	1	100–101	403.11	7.95	21.5	10	0	92	18	5	0	46	192.5
m4.4				**408.65**										
29A	95	1	41–42	411.67	12.90									
29A	95	2	26–27	413.02	13.45	17	15	0	123	13	5	3	72	248
29A	96	2	103–104	416.84	4.87	46	12	0	91	17	4	2	103	275
29A	101	1	128–129	430.84	4.20									
29A	101	2	37–38	431.43	3.86	56	10	-	83	26	6	0	91	272
29A	106	2	36–37	443.62	3.60									
29A	109	2	20–21	452.61	2.77	77	18	0	131	13	5	0	45	289
29A	113	1	102–103	464.13	2.09	106	5	2	143	15	8	0	48	327
29A	114	1	35–37	466.51	1.01	217.5	11	0	103	15	8	0	86	440.5
29A	117	2	60–61	477.41	2.03	107.5	12	0	144	10	8	1	56	338.5
m4.5				**478.61**										
29A	120	1	32–33	481.73	2.20									
29A	120	2	36–37	483.28	3.80	64	8	0	167	10	0	0	59	308
29A	121	1	113–114	485.08	3.10									
29A	126	1	100–101	500.71	1.39									

(*continued*)

TABLE 6. RATIOS OF NONSACCATE VERSUS BISACCATE POLLEN FROM INTEGRATED OCEAN DRILLING PROGRAM EXPEDITION 313 HOLES M0027A AND M0029A AND SUMMARY OF POLLEN DATA FROM HOLE M0027A (*continued*)

Hole	Core	Section	Depth in core	Depth mcd	Nonsac:Bisac	Bisac	TCT	Hemlock	Oak	Hickory	Elm	Palm	Other	Total
m5				**502.01**										
29A	128	3	73–74	508.79	3.00									
29A	129	1	70–71	509.56	0.03	112.5	15	0	122	29	2	1	72	353.5
29A	131	2	78–79	517.26	4.07	53.5	10	0	132	26	6	0	45	272.5
29A	132	2	30–31	519.81	3.20	71.5	24	1	96	34	3	0	72	301.5
29A	133	1	48–49	521.54	3.60									
29A	136	1	73–75	528.48	6.13									
29A	137	1	90–91	531.11	4.82									
29A	138	1	9–11	533.35	8.64	25	14	0	128	8	11	0	55	241
29A	139	1	24–26	536.56	4.59	47.5	14	0	143	13	3	0	45	265.5
29A	139	2	12–13	537.93	2.93	75.5	21	4	128	6	3	0	57	294.5
29A	144	1	29–30	551.85	9.20									
29A	145	1	133–134	555.94	5.02	44	15	1	14	14	4	0	53	265
29A	148	3	10–11	563.25	2.29									
29A	149	3	10–11	565.05	3.30									
29A	151	1	94–95	570.80	2.66	83.5	11	1	122	9	0	1	79	306.5
29A	151	3	17–18	573.43	3.03									
29A	154	2	90–91	581.45	8.19	26	26	0	74	12	4	1	97	241
29A	156	1	20–21	585.31	3.65									
29A	158	2	5–6	591.96	2.36									
29A	160	1	28–29	597.59	1.90									
m5.2				**602.25**										
29A				605.19	1.86	111.5	12	2	121	8	3	0	63	320.5
29A	165	2	154–156	615.64	5.60									
29A	167	2	21–22	619.54	1.30									
29A	168	1	21–22	621.92	3.83	60	8	0	129	17	11	1	65	291
29A	170	2	150–152	630.82	1.65									
29A	173	x	x	x	3.2									
29A	175	2	110–111	642.62	6.12	35.5	10	0	136	14	4	0	48	246.5
m5.3				**643.19**										
29A	176	1	76–77	643.82	1.70									
29A	179	1	5–6	650.99	1.40									
m5.4				**662.37**										
29A	183	1	110–111	662.81	1.47									
29A	183	2	110–111	663.81	5.17	42	15	0	137	15	10	0	44	263
29A	184	1	113–114	665.81	1.2									
29A	185	1		666.00	7.25									
m5.45				**673.71**										
29A	190	1	130–131	677.95	0.66									
29A	190	2	34–35	678.45	1.26									
29A	191	2	22–23	681.27	1.30									
29A	195	2	124–125	694.60	2.10									
m5.47				**696**										
29A	196	2	50–52	696.93	2.47	64.5	6	0	116	8	1	0	29	224.5
29A	199	2	46–47	706.02	2.89									
m5.6				**706.66–710**										
29A	204	1	145–147	717.71	7.62	29	17	0	117	30	1	0	38	250
29A	207	3	x	727.00	11.72	18.5	11	0	156	13	2	0	29	229.5
m5.7	x	x	x	**728.56**										
29A	209	1	111–112	732.62	0.98	258	55	25	103	24	3	0	43	511
29A	211	2	111–112	739.35	0.35									
m5.8	x	x	x	**746**										
29A	215	1	5–6	750.91	1.24									
29A	217	1	101–103	753.87	4.54									

Note: Nonsac:Bisac—nonsaccate vs. bisaccate pollen; mcd—meters composite depth; TCT—type cypress-cedar pollen.
*Prefixes m, O indicate sequences.

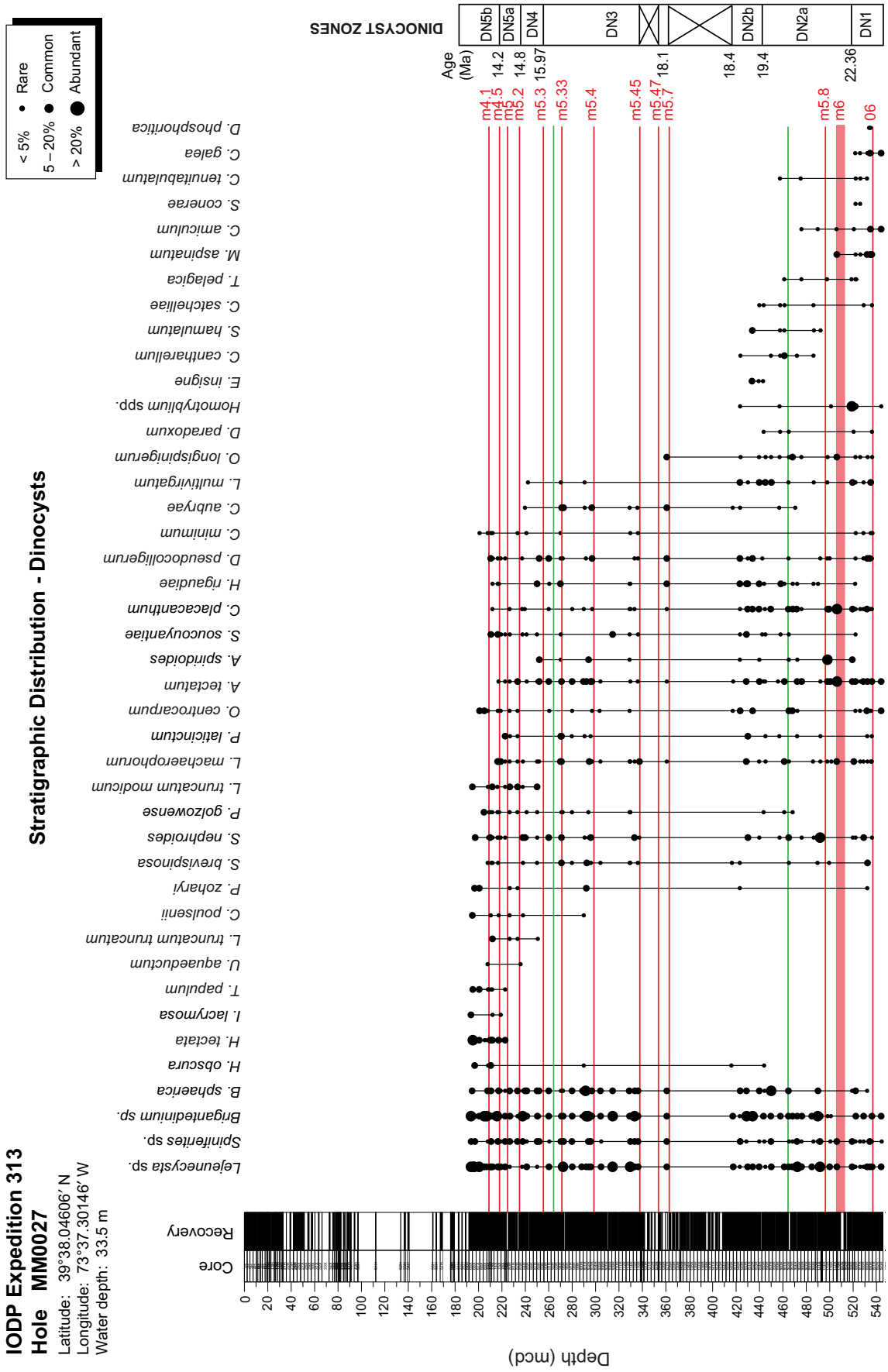

Figure 6. Semiquantitative depiction of the stratigraphic distribution of selected ubiquitous and age-diagnostic dinocysts in Integrated Ocean Drilling Program Hole 27A (raw data available in Supplemental Table 1 [see footnote 1]). Red lines represent sequence-bounding unconformities (depths of impedance contrasts follow Miller et al., 2013a). Zones are based on de Verteuil and Norris (1996), as depicted in Figure 2 and discussed in the text, and ages of zone boundaries are calibrated to the Gradstein et al. (2004) time scale. Depth: mcd—meters composite depth; mbsf—meters below seafloor. Useful datums are listed in Table 1.

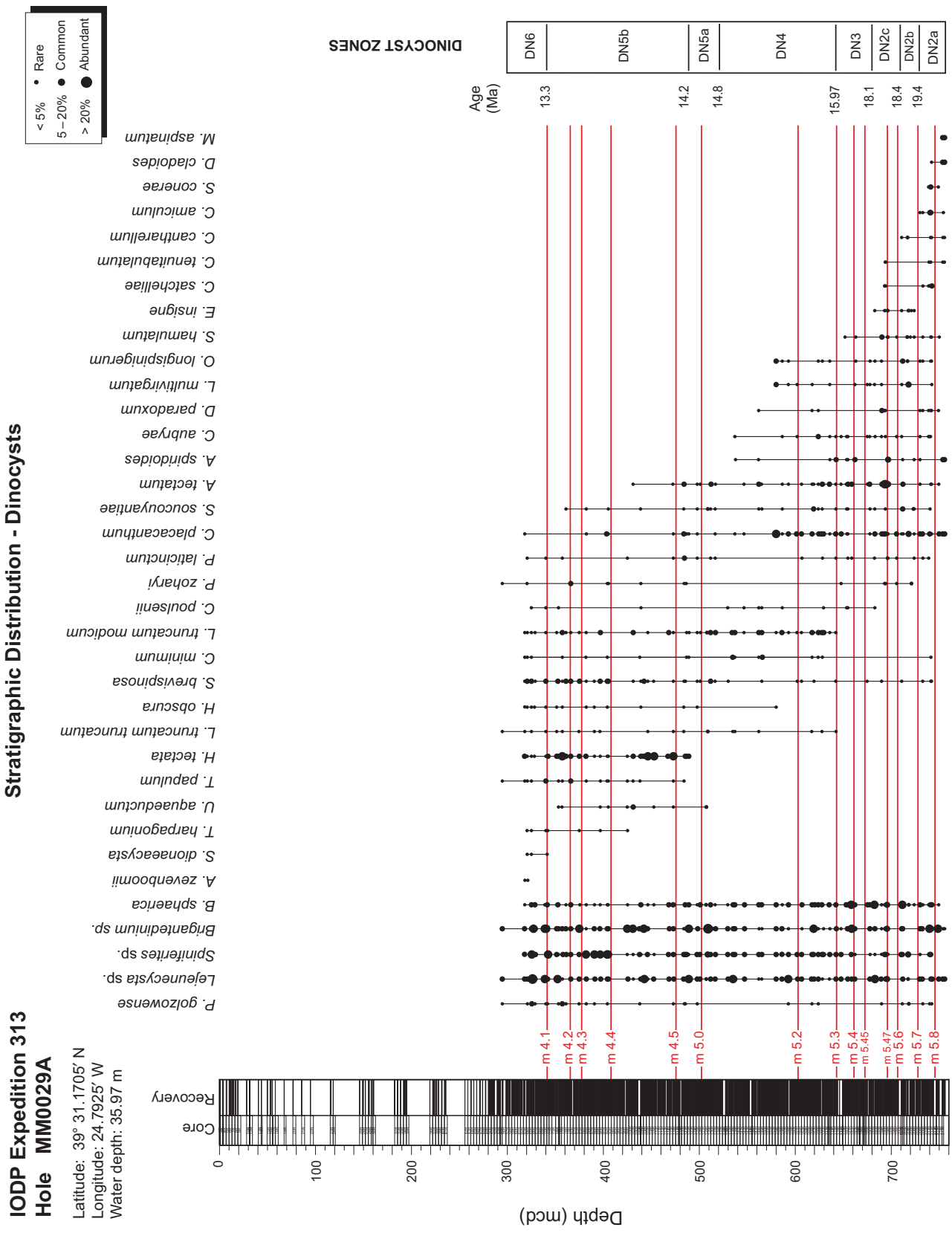

Figure 7. Semiquantitative depiction of the stratigraphic distribution of selected ubiquitous and age-diagnostic dinocysts in Integrated Ocean Drilling Program Hole 29A (raw data available in Supplemental Table 2 [see footnote 2]). Depth: mcd—meters composite depth. Red lines represent seismic reflectors interpreted as sequence-bounding unconformities (depths of impedance contrasts follow Miller et al., 2013a). Zones are based on de Verteuil and Norris (1996) as depicted in Figure 2, and ages of zone boundaries are calibrated to the Gradstein et al. (2004) time scale. Useful datums are listed in Table 2.

Lithologic Unit VI: Sequence m5.8

G:P values are typically relatively low in sequence m5.8 at both sites where characteristic dinocyst taxa in include *Lejeunecysta* spp., *Brigantedinium* spp., *Cleistosphaeridium placacanthum*, *Batiacasphaera sphaerica*, *Dapsilidinium pseudocolligerum*, *Apteodinium tectatum*, *Apteodinium spiridoides*, *Operculodinium longispinigerum*, *Hystrichokolpoma rigaudiae*, *Cousteaudinium aubryae*, *Distatodinium paradoxum*, and *Paleocystodinium* sp. (Figs. 6, 7, and 8; Tables 1 and 2; Supplemental Tables 1 and 2 [see footnotes 1 and 2]). This assemblage is similar to that reported by de Verteuil and Norris (1996) in their Sumatradinium soucouyantiae interval zone found in the Early Miocene Popes Creek Sand Member of the Calvert Formation of Maryland and Virginia (equivalent to the lower Kirkwood Formation of New Jersey). Several biostratigraphically important Early Miocene taxa have their HO in sequence m5.8 at both sites (Figs. 6 and 7; Tables 1 and 2), e.g., *Caligodinium amiculum*, *Cribroperidinium tenuitabulatum*, and *Dinopterigium cladoides*. This is consistent with other chronological indicators that bracket the age of this sequence between 20.2 and 19.2 Ma,

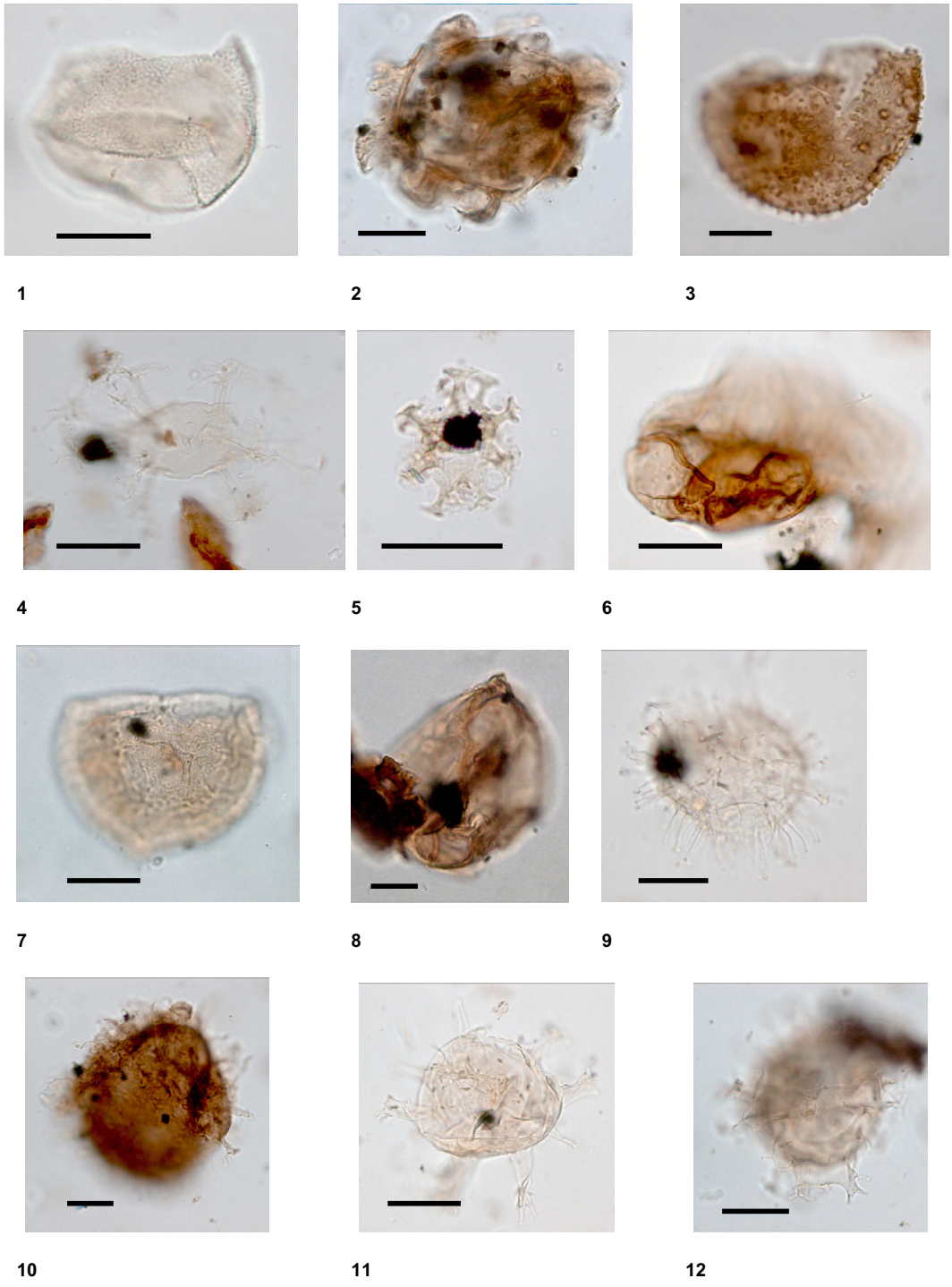

Figure 8. Common marine palynomorphs in sequence m5.8 (lower Burdigalian, dinoflagellate zones DN2a, DN2b), including species, sample number, depth (in parentheses), and England Finder coordinates. (1) *Batiacasphaera sphaerica* Stover 1977: 313–29A-211R1 (31–32 cm), M54/4-N58/1. (2) *Cordosphaeridium cantharellus* (Brosius) Sarjeant, 1981: 313–29A-208R2 (44–45 cm), F55/0–1. (3) *Cerebrocysta satchelliae* de Verteuil and Norris 1996: 313–29A-208R2 (44–45 cm), T71/2. (4) *Distatodinium paradoxum* (Brosius) Eaton, 1976: 313–29A-208R2 (44–45 cm), W38/1–3. (5) *Cordosphaeridium minimum*: 313–29A-208R2 (44–45 cm), N43/0–3. (6) *Cousteaudinium aubryae* de Verteuil and Norris 1996: 313–29A-211R1 (31–32 cm), P57–0. (7) *Stoverocysta conerae* Biffi and Manum 1988: 313–29A-208R2 (44–45 cm). (8) *Cribroperidinium tenuitabulatum* (Gerlach) Helenes 1984: 313–27A-165R-CC; 10. (9) *Cleistosphaeridium placacanthum*: 313–29A-211R1 (31–32 cm). (10) *Sumatradinium soucouyantiae* de Verteuil and Norris 1992: 313–29A-208R2 (44–45 cm), R67/2. (11) *Hystrichokolpoma rigaudiae* Deflandre and Cookson 1955: 313–29A-211R1 (31–32 cm), P67–1. (12) *Spiniferites mirabilis* (Rossignol) Sarjeant: 313–29A-212R1 (38–39 cm), N36/0–3.

lowermost Burdigalian, i.e., calcareous nannofossils assigned to upper zone NN2 (Browning et al., 2013). The HO of *Caligodinium amiculum* (in sample 27A-164R-2, 110–111 cm, 470.46 mcd) and the lowest occurrence (LO) of *Exochosphaeridium insigne* (in sample 27A-156R-1, 18–19 cm, 445.14 mcd) occur within the thick sequence m5.8 in Hole 27A, marking the boundary between subzones DN2a and DN2b, ca. 19.5 Ma (Fig. 6; Table 1) In contrast, *Caligodinium amiculum* is present throughout the much thinner sequence in Hole 29A and *Exochosphaeridium insigne* is not present (Fig. 7; Table 2), suggesting that sequence m5.8 is truncated at Site 29.

Terrestrial palynomorphs generally dominate assemblages in sequence m5.8 at both sites, with T:M between 1.37 and 20.90 (mean 5.68, n = 32) in the thick sequence in Hole 27A, and between 1.15 and 11.82 (mean 3.91, n = 7) in the more distal Hole 29A (Fig. 5). Pollen assemblages in Hole 27A are dominated by *Quercus* (oak) and *Carya* (hickory), with highly variable concentrations of bisaccate pollen (nonsac:bisac ranges 0.59–20.09, mean = 6.85, n = 36 in Hole 27A; Fig. 3; Table 6). Several peaks (~3%–12%) in inaperturate (TCT, i.e., type cypress-cedar) conifer pollen in sequence m5.8 are probably related to development of coastal wetlands during the early Burdigalian. There is a peak in *Tsuga* (hemlock) in Hole 29A that is apparently not represented in Hole 27A, possibly correlating with the barren sandy sediments at the top of the sequence at this neritic site. The palynofacies vary from rich in AOM (type 2) to very rich in phytoclasts (type 1) in the thick sequence m5.8 at Site 27 (Fig. 3; Table 5), with an increase in phytoclast abundance upsequence, particularly above ~465 mcd. It is in this sequence that phytoclasts first become an abundant component of the palynofacies in Hole 27A, first exceeding AOM in sample 27A-169R-1 (32–33 cm, 484.93 mcd; Figs. 3 and 5; Table 5). Phytoclasts also exceed AOM in the three samples quantitatively analyzed for palynofacies in the thin sequence m5.8 in Hole 29A (mean Ph:AOM = 2.28, range 1.12–3.02; Figs. 4 and 5; Table 5), suggesting that the thin sequence m5.8 in Hole 29A does not correlate with the oldest sediments in this sequence in Hole 27A, which are still AOM dominated. These indications of increased terrigenous flux are consistent with the presence of unfossiliferous sands in the upper 50 m of lithologic unit VI in Hole 27A. Bisaccate conifer pollen continues to dominate the pollen assemblage in several samples analyzed from this sequence in Hole 29A, recording continued dominance of long-distance transport (Table 6).

Lithologic Unit V: Sequence m5.7

Common dinocyst taxa in sequence m5.7 at both sites include *Batiacasphaera sphaerica*, *Cleistosphaeridium placacanthum*, *Apteodinium tectatum*, *Dapsilidinium pseudocolligerum*, *Operculodinium centrocarpum*, *Operculodinium longispinigerum*, and *Hystrichokolpoma rigaudiae* (Figs. 6 and 7; Supplemental Tables 1 and 2 [see footnotes 1 and 2]). The sparse phytoclast-dominated assemblage very rich in terrestrial palynomorphs in the two samples analyzed from Hole 27A precludes a more definitive age assignment than DN2–top DN4. This is not surprising, given the extraordinarily high abundances of fungal spores in the two samples analyzed from Hole 27A that record an exceptionally strong terrestrial influence. In sample 29A-204R-1 (145–147 cm, 717.71 mcd), however, *Exochosphaeridium insigne* co-occurs with *Cordosphaeridium cantharellus* (Fig. 7; Table 2), constraining these sediments to DN2b (ca. 19.5–18.4 Ma). This is consistent with a single calcareous nannofossil assignment of upper zone NN2 (Browning et al., 2013).

G:P is high in this sequence, 2.8 and 5.0 in the 2 samples from Hole 27A and ranging from 2.07 to 7.89 in Hole 29A, although protoperidinioid taxa are common in some samples (primarily the ubiquitous *Lejeunecysta* and *Brigantedinium* spp., but also including lower concentrations of *Sumatradinium soucouyantiae* and *Palaeocystodinium* spp., primarily *P. golzowense*). AOM dominates the palynofacies in sequence 5.7 in Hole 29A where T:M values are relatively low, averaging ~3.09 (range 1.60–4.39, n = 7), and palynomorphs are abundant (mean 149,100, range 64,500–230,000 palynomorphs/cm^3), suggesting low rates of sediment accumulation at the distal site. Samples are assigned to palynofacies type 2 or type 3 of Batten (1996) in Hole 29A, whereas sequence m5.7 samples in Hole 27A are very rich in phytoclasts and other terrigenous components and are assigned to palynofacies type 1 (Table 5). Bisaccate pollen is rare within this sequence in Hole 29A (Fig. 4; Table 6), however, with *Quercus* remaining the dominant pollen type, paired with particularly high percentages of *Carya* in some samples. This suggests that a real change in vegetation occurred during the early Burdigalian, with an expansion of broadleaf deciduous trees at the expense of evergreen conifers. T:M ratios were 15.72 and 10.50 in the 2 samples analyzed from this thin, sandy sequence in Hole 27A (27A-127R1, 15–16 cm, 359.71 mcd), recording much more proximal conditions at Site 27, consistent with the seismic and sedimentological data (Figs. 3–5).

Lithologic Unit V: Sequence m5.6

Sequence m5.6 was not resolved at Site 27, but *Exochosphaeridium insigne* is present through sequence m5.6 (HO in sample 29A-195R-1, 50–51 cm, 692.36 mcd; Fig. 7; Table 2). The HO of *Cordosphaeridium cantharellus* in sample 29A-196R-2 (96.93 mcd; Fig. 7; Table 2) identifies the subzone DN2b-DN2c boundary, which straddles the NN2-NN3 boundary, ca. 18.4 Ma (Fig. 2). This is consistent with other chronological proxies that constrain the age of this sequence to between 18.4 and 18.1 Ma: a single assignment to zone NN3 and an Sr isotope age of 17.9 Ma (Browning et al., 2013). Other common dinocysts in this sequence include *Operculodinium centrocarpum*, *Apteodinium tectatum*, *Dapsilidinium pseudocolligerum*, *Cleistosphaeridium placacanthum*, *Batiacasphaera sphaerica*, *Spiniferites* spp., *Polysphaeridium zoharyi*, *Pentadinium laticinctum*, and *Homotryblium* spp. (Fig. 7; Supplemental Table 2 [see footnote 2]). *Lejeunecysta* spp. are the only common protoperidinioid cysts and G:P values are high (G:P ranges from 3.92 to 6.89 in the 3 samples analyzed for dinocysts). T:M values remain relatively low, averaging 2.89 (range 1.72–4.38, n = 3; Figs. 4 and 5; Table 4) and bisaccate pollen are relatively abundant (nonsac:bisac average 2.3; Fig. 4; Table 6), and pollen of taxa associated with wet conditions and/or swamps decrease in abundance relative to sequence m5.7. Amorphous organic matter dominates samples in this sequence, assigned to palynofacies type 3 of Batten (1996) (Table 5).

Lithologic Unit V: Sequence m5.47

In Hole 27A the thin, sandy sequence m5.47 is barren of palynomorphs except for a single sample at the top of the sequence (27A-116R-2, 38–39 cm, 337.04 mcd), although AOM is relatively abundant, with most samples assigned to palynofacies type 2 (Table 5). Palynomorphs were recovered from every sample examined from this sequence in Hole 29A (mean 63,900, range 16,100–112,800 palynomorphs/cm^3). *Cousteaudinium aubryae*, *Lingulodinium multivirgatum*, *Operculodinium longispinigerum*, *Batiacasphaera sphaerica*, *Spiniferites* sp., *Polysphaeridinium zoharyi*, and *Cleistosphaeridium placacanthum* are consistently present; this is an assemblage similar to the Cousteadinium aubryae interval zone of de Verteuil and Norris (1996) found in the Fairhaven Member of the Calvert Formation. The LO of *Cerebrocysta poulsenii* in sample 29A-191R-2 (22–23 cm, 681.27 mcd) and of *Sumatradinium druggii* in sample 29A-194R-2 (23–24 cm, 660.55 mcd) together with dinocyst taxa having an HO in the Early Miocene (e.g., *Lingulodinium multivirgatum* and *Operculodinium longispinigerum*)

allows us to assign these sediments to DN3 (18.1–15.97, upper Burdigalian) (Fig. 7; Table 2). This assignment is younger than the diatom zonation suggests, but is consistent with the nannofossil assignment to zone NN4 (Browning et al., 2013). T:M values remain low in Hole 29A (Figs. 4 and 5; Table 4), averaging ~2.75 (range 1.59–5.15, n = 10) and bisaccate pollen is abundant (mean nonsac:bisac ~1.27, range 1.22–1.3; Fig. 4; Table 6), with *Quercus* dominating the nonsaccate pollen assemblage. The interpretation of high sea level is consistent with the continued dominance of AOM, with Ph:AOM ranging from 0.04 to 0.27 in Hole 29A where most samples were assigned to palynofacies type 3 (Table 5).

Lithologic Unit IV: Sequence m5.45

All of the palynological proxies record a sharp increase in terrigenous flux to the New Jersey margin within lithologic unit IV. The ratio of Ph:AOM rises sharply in the upper part of sequence m5.45 in Hole 27A in samples mostly assigned to palynofacies type 1, exceeding 100:1 in sample 27A-105R-CC (304.95 mcd), and the strongest T:M peak in all of the samples studied was found higher up in this sequence (T:M = 43.25 in sample 27A-104R-3, 36–38 cm, 301.86 mcd) (Figs. 3 and 5; Table 3). Terrigenous flux to Hole 27A is high through this sequence, with mean T:M = 8.85, n = 7 (Fig. 3). At the more distal Site 29, there is an increase in Ph:AOM (Fig. 4; Table 5), although AOM continues to dominate (palynofacies type 2), and the ratio of terrestrial versus marine palynomorphs in sequence m5.45 (mean T:M = 4.86, range 2.74–7.05, n = 4; Figs. 4 and 5; Table 4) is higher than the Miocene average for this site (T:M = 3.82). Increased (possibly fluvial) terrigenous flux is also consistent with the diverse angiosperm-dominated assemblage that characterizes both holes; large heavy grains of *Carya* and *Ulmus* (elm) are especially abundant, in addition to the ubiquitous *Quercus*. Peak warmth on the New Jersey margin is recorded by the presence of Arecaceae/*Arecipites*-type (palm) pollen in this sequence, as well as in the overlying composite sequence m5.4. Palynological evidence of a sharp increase in terrigenous flux, particularly to the more proximal Site 27, is consistent with the seismic profile that shows that the clinoform break migrated past the site of corehole 27A at that time (Fig. 5; see also Browning et al., 2013, fig. 2 therein).

G:P values are relatively low in sequence m5.45 (ranging from 0.67 to 2.62 in Hole 27A and 2.77 to 3.17 in Hole 29A; Figs. 3 and 4), recording neritic conditions and/or high productivity and/or high rates of sedimentation. Common to abundant protoperidinioid taxa include *Brigantedinium* spp., *Lejeunecysta* spp., *Echinidinium* spp. *Selenopemphix nephroides*, *Selenopemphix brevispinosa*, *Palaeocystodinium* spp. and *Sumatradinium soucouyantiae* (Figs. 6 and 7; Supplemental Tables 1 and 2 [see footnotes 1 and 2]). *Cousteaudinium aubryae* is also consistently present in this sequence, as are gonyaulacoid cysts *Batiacasphaera sphaerica*, *Apteodinium tectatum*, *Apteodinium spiridoides*, *Cleistosphaeridium placacanthum*, and *Lingulodinium machaerophorum*. This assemblage, in the absence of diagnostic Middle Miocene taxa, allows us to assign this sequence to DN3 (18.1–15.97 Ma, upper Burdigalian), which is consistent with better constrained dinocyst zonation of the underlying sequence m5.47 and with the assignment to nannofossil zone NN4 and the Sr age of 17.7 Ma. These ages are younger than the diatom zonation suggests (Browning et al., 2013), but are consistent with oxygen isotope and other proxies recording warm, humid conditions between ca. 18 and 16.5 Ma (Middle Miocene Climatic Optimum; Zachos et al., 2001).

Lithologic Unit III: Sequence m5.4

In Miller et al. (2013b), seismic profiles, core data, and log stacking patterns were used to recognize that sequence m5.4 is a composite of three higher order (100–400 k.y. scale) sequences called m5.4–1 (the sequence that directly overlies surface m5.4), m5.34, and m5.33. At Hole M27A, sequences m5.34 and m5.33 are recognized in a topset setting, but sequence m5.4–1 is cut out. At Site M29, seismic resolution did not permit the higher order sequences to be defined in this bottomset setting and the section there is referred to as m5.4 (Miller et al., 2013b).

The continued presence of Arecaceae/*Arecipites*-type (palm) pollen in a diverse angiosperm pollen flora with relatively high percentages of *Ulmus* records continued warm, humid conditions in the New Jersey hinterland (Table 5). G:P remains relatively low in sequence m5.4 in Hole 27A (mean G:P = 1.76, range 0.73–2.76, n = 5; Fig. 3; Table 3), where a diverse protoperidinioid cyst assemblage includes *Selenopemphix brevispinosa*, *Selenopemphix nephroides*, *Palaeocystodinium* spp., *Sumatradinium soucouyantiae*, *Echinidinium* spp., and *Lejeunecysta* spp. in addition to the ubiquitous *Brigantedinium* spp. (Supplemental Table 1 [see footnote 1]). Higher G:P values characterize the more distal Hole 29A (mean G:P = 2.91, range 1.23–4.51, n = 4; Fig. 4; Table 4). T:M values are variable, but higher than the Miocene average at both sites, ranging from ~2.09 to 15.0 (mean ~5.99, n = 6) in Hole 27A and from ~1.63 to 12.76 (mean ~4.67, n = 6) in Hole 29A (Figs. 3 and 4; Tables 3 and 4). The strongest T:M peak in Hole 29A (T:M = 12.76) is at the base of this sequence, in sample 29A-182R-2 (99–100 cm, 660.81 mcd), and a very high T:M peak (15.00) was found in sample 27A-101R-CC (292.8 mcd). The palynofacies in Hole 27A is dominated by phytoclasts (palynofacies type 1 of Batten, 1996), especially at the base of this sequence where T:M is very high, but AOM remains common in this sequence in Hole 29A, with Ph:AOM values similar to those in the underlying sequence m5.45 (Figs. 3 and 4; Table 5).

Sequence m5.4 contains common *Batiacasphaera sphaerica*, *Apteodinium tectatum*, *Cleistosphaeridium placacanthum* and *Lingulodinium machaerophorum* together with *Apteodinium spiridoides* and *Cousteaudinium aubryae*. The LO of *Labyrinthodinium truncatum modicum* and *Labyrinthodinium truncatum truncatum* (and thus the base of DN4, 15.97 Ma; Figs. 6 and 7; Tables 1 and 2) occur at the top of this sequence in Hole 29A in sample 29A-176R-1 (76–77 cm, 643.82 mcd), although these useful Middle Miocene markers are not found until the base of sequence m5.3 in Hole 27A (in sample 27A-88R-2, 110–111 cm, 252.86 mcd). Most of sequence m5.4 in Hole 29A, and all of this sequence in Hole 27A, is thus assigned to DN3, which is consistent with all other chronostratigraphic proxies (Browning et al., 2013).

Lithologic Unit III: Sequence m5.33

Sequence m5.33, which forms the upper part of lithologic unit III Hole 27A but is not present in Hole 29A, contains a dinocyst assemblage similar to that in sequence m5.4, but gonyaulacoid cysts dominate, with G:P values averaging 4.81 (Fig. 3; Table 3). The dinocyst assemblage is rich in *Batiacasphaera sphaerica*, *Cleistosphaeridium placacanthum*, *Lingulodinium machaerophorum*, *Apteodinium tectatum*, and *Apteodinium spiridoides* (Fig. 6; Supplemental Table 1 [see footnote 1]). The HO of *Lingulodinium multivirgatum* occurs in this sequence, in sample 313–27A-94R-2 (100–101 cm, 270.56 mcd; Fig. 6; Table 1), allowing this sequence to be assigned to DN3.

A relatively diverse oak-dominated angiosperm pollen assemblage continues to characterize this sequence (Table 5), but the presence of *Fagus*/*Nyssa* (beech/tupelo, or black gum) and the absence of Arecaceae/*Arecipites*-type (palm) pollen record climatic cooling. AOM is common in this sequence (Table 5), recording a decrease in terrigenous flux. This is consistent with the relatively low T:M values in this sequence, averaging ~3.9 (range 1.9–6.15, n = 3; Figs. 3 and 5; Table 3).The palynological assemblage thus records a distal setting around 15.97 Ma (the Burdigalian-Langhian boundary).

Lithologic Unit II: Sequence m5.3

Palynomorphs are relatively sparse in sequence m5.3 (averaging ~20,589 palynomorphs/cm^3 in Hole 27A and ~16,593 palynomorphs/cm^3 in Hole 29A). The palynofacies is generally rich in AOM (Figs. 3–5; Table 5), and the remains of marine protozoans (e.g., radiolarians and foraminifer linings) are common (palynofacies type 2 of Batten, 1996). T:M values are very low in Hole 27A, averaging only 2.66 (range 1.06–6.31, n = 5) above the sequence boundary in sample 27A-88R-2 (110–111 cm, 252.86 mcd), where T:M was 6.31 (Figs. 3 and 5; Table 3). T:M values are also low in Hole 29A, averaging ~3.05 (range 1.57–8.00, n = 8). G:P is very high in Hole 29A, averaging 5.45 (n = 7), reaching a peak of 15.33 in sample 29A-170R-2 (150–152 cm, 630.82 mcd; Figs. 4 and 5; Table 4). G:P is also very high in the lower part of the sequence in Hole 27A, reaching 12.00 in sample 313–27A-88R-2 (100–101 cm, 252.86 mcd), but protoperidinioids outnumber gonyaulacoid cysts in the upper part of this sequence (in samples 27A-84R-2, 41–42 cm, 239.47 mcd and 27A-83R-3, 11–102 cm, 237.52 mcd; Fig. 3; Table 3). The relatively low diversity pollen assemblages are generally dominated by *Quercus* (Table 5). The palynological proxies all record more distal conditions during the early Langhian than existed in the late Burdigalian (recorded in sequences m5.45–m5.4).

The LO of *Labyrinthodinium truncatum modicum* in sample 27A-88R-2 (110–111 cm, 252.86 mcd), together with the LO of *Labyrinthodinium truncatum truncatum* and *Impagidinium arachnion* in sample 27A-88R-1 (50–51 cm, 250.26 mcd; Fig. 6; Table 1), allows us to assign this sequence to DN4 (15.97–14.8 Ma), an age consistent with all other chronostratigraphic proxies (Browning et al., 2013). As de Verteuil and Norris (1996) reported, the assemblage in their Distatodinium paradoxum interval zone differs primarily from the underlying Cousteaudinium aubryae interval zone in containing *Labyrinthodinium truncatum*. Gonyaulacoid dinocysts such as *Batiacasphaera sphaerica*, *Cleistosphaeridium placacanthum*, *Dapsilidinium pseudocolligerum*, and *Apteodinium tectatum* generally dominate the assemblage together with *Labyrinthodinium truncatum modicum*. *Lejeunecysta* spp. and *Brigantedinium* spp. are common to abundant in several samples, and other protoperidinioid cysts such as *Echinidinium* spp., *Palaeocystodinium* spp., *Selenopemphix brevispinosa*, *Selenopemphix nephroides*, *Sumatradinium druggii*, and *Sumatradinium soucouyantiae* are also usually present to common (Figs. 6 and 7; Supplemental Tables 1 and 2 [see footnotes 1 and 2]). This assemblage allows sequence m5.3 to be assigned to DN4, an age consistent with all other chronostratigraphic proxies.

Lithologic Unit II: Sequence m5.2

Palynomorph concentrations remain low in sequence m5.2 in Hole 27A, averaging 30,950 palynomorphs/cm^3. Mean concentrations in Hole 29A are ~125,600 palynomorphs/cm^3, exhibiting a wide range (22,900–381,900 palynomorphs/cm^3) with the concentration peaks generally characterized by relatively high T:M (>4; Figs. 3 and 4). T:M values average ~3.10 (range 1.28–5.92, n = 29) in the thick sequence in Hole 29A and T:M is 1.48 and 1.59 in the two samples analyzed from this very thin sequence in Hole 27A. A relatively diverse angiosperm pollen assemblage characterizes sequence 5.2 (with relatively high percentages of *Tilia*, *Ulmus*, and *Fagus* pollen compared to *Quercus* in Hole 29A), although bisaccate grains tend to increase in relative abundance upcore through this sequence, culminating in ~30% of total pollen at the sequence m5 boundary (Figs. 3 and 4; Table 6). Inaperturate conifer TCT pollen shows particularly high abundances in the lower part of this sequence, perhaps recording the expansion of cypress swamps on the Atlantic coastal plain associated with the Middle Miocene Climate Optimum (see Browning et al., 2013; Fig. 7). *Labyrinthodinium truncatum modicum* and *Labyrinthodinium truncatum truncatum* are both consistently present together with *Batiacasphaera sphaerica*, *Apteodinium tectatum*, *Dapsilidinium pseudocolligerum*, *Cleistosphaeridium placacanthum*, *Lingulodinium machaerophorum*, and *Cordosphaeropsis minimum* (Figs. 6, 7, and 9; Supplemental Tables 1 and 2 [see footnotes 1 and 2]). Protoperidinioid cysts like *Selenopemphix brevispinosa*, *Selenopemphix nephroides*, *Sumatradinium soucouyantiae*, *Echinidinium* spp., and *Palaeocystodinium* spp. are present in variable quantities in these sediments in addition to the ubiquitous *Lejeunecysta* and *Brigantedinium* spp. The HO of *Apteodinium spiridoides* at the base of this sequence in sample 27A-88R-2 (110–111 cm, 252.16 mcd; Fig. 6; Table 1) may represent reworking, but the LO of *Unipontedinium aquaeductum* in samples 27A-83R-3 (11–12 cm, 237.62 mcd) and 29A-128R-3 (73–74 cm, 508.79 mcd) at the top of this sequence at both sites (Tables 1 and 2; Figs. 6 and 7) marks the DN4-DN5 boundary. Exceptionally high abundances of the acritarch *Cyclopsiella granosa* (typically found in shallow-marine and/or nearshore high-energy environments according to Louwye and Laga, 2008) at the top of this sequence in Hole 29A appears to record a dramatic increase in fluvial flux or substantial downslope mass wasting and resedimentation, consistent with the geometry of the margin at the time (Fig. 5).

Lithologic Unit II: Sequence m5

The palynological proxies continue to record distal conditions in sequence m5. In both holes, sequence m5 is characterized by assemblages rich in AOM (palynofacies type 2 of Batten, 1996; Figs. 3–5; Table 6). Bisaccate conifer pollen is relatively abundant, and the lower part of sequence m5 is characterized by particularly low percentages of hickory pollen (*Carya*), reflecting the cooling that marks the early Serravallian (event Mi3; see Browning et al., 2013, fig. 7 therein). T:M values are very low in Hole 29A (mean T:M = 2.89, range 2.28–3.50, n = 4) but substantially higher in the two samples analyzed from this very thin sequence in Hole 27A (mean T:M = 4.58, range 3.69–5.46, n = 2; Figs. 3–5; Tables 3 and 4). The much lower palynomorph abundances in Hole 29A than in Hole 27A suggest that most terrigenous flux is not reaching the bottomsets (mean palynomorph concentration is only ~48,600/cm^3, range 25,600–80,300 palynomorphs/cm^3 in Hole 29A whereas it is ~133,600 palynomorphs/cm^3 in Hole 27A, increasing sharply upcore from ~44,000 to 244,000 palynomorphs/cm^3) (Figs. 3 and 4).

G:P values are relatively low at both sites, with common protoperidinioid cysts including *Lejeunecysta* spp. *Brigantedinium* spp. *Sumatradinium soucouyantiae*, *Sumatradinium druggii*, *Selenopemphix brevispinosa*, *Palaeocystodinium* spp., and *Trinovantedinium* spp., mainly *Trinovantedinium papulum* (Figs. 6 and 7; Supplemental Tables 1 and 2 [see footnotes 1 and 2]). The LO of *Habibacysta tectata* and the last common occurrence of *Apteodinium tectatum* occur within this sequence in both holes (Tables 1 and 2; Figs. 6 and 7), marking the boundary between zones DN5a and DN5b, ca. 14.2 Ma. This is consistent with age estimates based on other available proxies (Browning et al., 2013). The most distinctive feature of this sequence is an acme of *Pentadinium laticinctum* in both holes (sample 313–29A-119R-CC, where these cysts make up nearly 20% of the assemblage, and sample 27A-77R-2 [40–41 cm, 221.11 mcd], where they make up nearly 10% of the assemblage; Supplemental Tables 1 and 2 [see footnotes 1 and 2]). Other consistently present gonyaulacoid cysts include *Batiacasphaera sphaerica*, *Lingulodinium machaerophorum*, *Cleistosphaeridium placacanthum*, *Dapsilidinium pseudocolligerum*, *Hystrichosphaeropsis obscura*, and *Polysphaeridium zoharyi*.

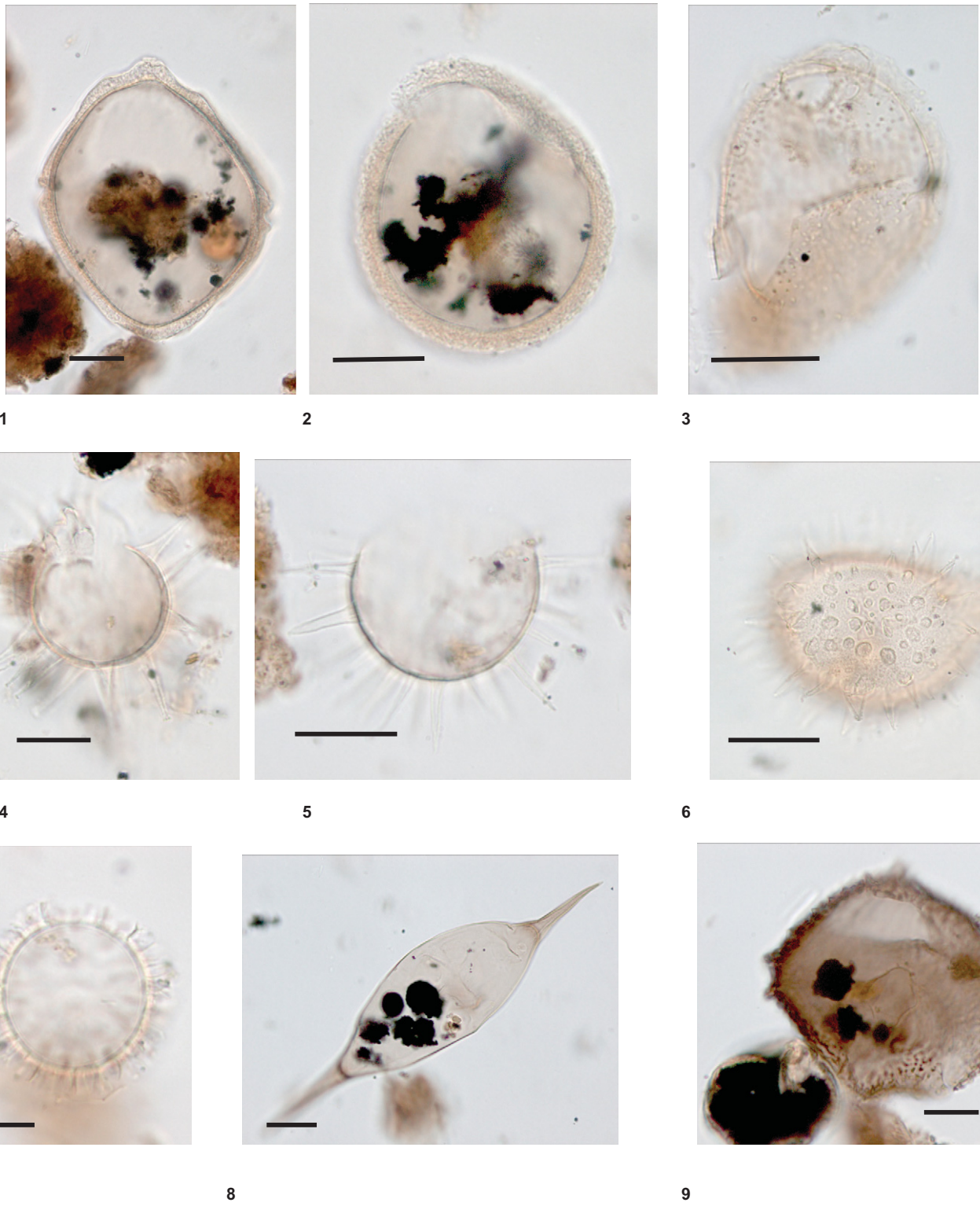

Figure 9. Common marine palynomorphs in sequence m5.2 (upper Langhian–lower Serravallian, dinoflagellate zones DN4–DN5a) including species, sample number, and England Finder coordinates. Depth for each = 15–16 cm. (1) *Apteodinium tectatum* Piasecki 1980: 313–29A-126R1, U53/3- V53/1. (2) *Tectatodinium pellitum* Wall, 1967: 313–29A-126R1, X52–1. (3) *Cyclopsiella granosa /elliptica*: 313–29A-126R1, C37/2. (4) *Dapsilidinium pseudocolligerum* (Stover) Bujak et al. 1980: 313–29A-126R1, R61–0. (5) *Lingulodinium machaerophorum* (Deflandre and Cookson) Wall, 1967: 313–29A-126R1, v48/4-V49/3. (6) *Lingulodinium multivirgatum* de Verteuil and Norris, 1996: 313–29A-126R1, N62–1. (7) *Labyrinthodinium truncatum* ssp. *modicum* de Verteuil and Norris 1996: 313–29A-126R1, R61–0. (8) *Palaeocystodinium golzowense* Alberti, 1961: 313–29A-126R1, X60–0. (9) *Trinovantedinium* sp.1: 313–29A-126R1, G64–3.

Lithologic Unit II: Sequence m4.5

Palynomorphs increase sharply in abundance within sequence m4.5 in Hole 29A, where they average 107,400 palynomorphs/cm^3 (range 39,500–217,000 palynomorphs/cm^3), but palynomorph concentrations in the thin sequence in Hole 27A average only ~67,400 palynomorphs/cm^3, declining sharply in abundance upcore. It is surprising that T:M values in sequence m4.5 in Hole 27A are lower than in Hole 29A (Hole 27A: mean ~1.96, range 1.27–3.50, n = 6; Hole 29A: mean ~5.18, range 0.56–11.17, n = 14); this suggests that most terrigenous flux is bypassing the more neritic site, an interpretation consistent with the geometry of this sequence (Fig. 5). This is also consistent with the dominance of phytoclasts through much of this sequence in Hole 29A, and the first sample with Ph:AOM > 40 at 421.26 mcd (sample 29A-89R-2, 70–71 cm; Table 5), although most samples from Hole 27A were assigned to palynofacies type 2 of Batten (1996) (Table 5). Cool early Serravallian conditions are recorded by high relative abundances of bisaccate pollen in both holes, with nonsac:bisac values ranging from 2.64 to 5.06 in Hole 27A and from 1.01 to 4.87 in the lower part of sequence m4.5 in Hole 29A (Table 6).

G:P values are relatively low in sequence m4.5 in Hole 27A (range 1.15–2.54) and in the upper part of this sequence in Hole 29A above a silty sand, where G:P values reach a peak of 13.00 in sample 29A-109R-2 (20–21 cm, 452.61 mcd; above this silty sand, G:P ranges from 0.44 to 2.67; Figs. 3 and 4; Tables 3 and 4). Low G:P suggests lower than normal marine salinity and high nutrient flux (i.e., fluvial influence) during the latest Langhian, consistent with the sharp increase in phytoclasts versus AOM and the rapid progradation evident in Figure 5. In addition to *Lejeunecysta* spp. and *Brigantedinium* spp., *Habibacysta tectata* is common to abundant, and other common dinocyst taxa include *Spiniferites* spp., *Batiacasphaera sphaerica*, *Lingulodinium machaerophorum*, *Selenopemphix brevispinosa*, *Selenopemphix nephroides*, *Dapsilidininium pseudocolligerum*, *Labyrinthodinium truncatum modicum*, and *Sumatradinium soucouyantiae* (Supplemental Tables 1 and 2 [see footnotes 1 and 2]). This assemblage is assigned to DN5b, consistent with ages derived from other proxies (Browning et al., 2013).

Lithologic Unit II: Sequences m4.4–m4.2

Sequences m4.4–m4.2 were not resolved in Hole 27A. In Hole 29A, T:M values are relatively low but rise slowly in sequences m4.4–m4.2: sequence m4.4 (mean ~2.35, range 1.30–4.14, n = 7 in Hole 29A), T:M ~2.45; T:M = 3.43 in the 2 samples analyzed from sequence m4.3; and mean T:M = 3.79 (range 2.27–6.72, n = 6) in sequence m4.2. A diverse angiosperm pollen assemblage characterizes these sequences that are rich in phytoclasts, although AOM remains common in some samples (palynofacies types 1 and 2 of Batten, 1996) (Tables 5 and 6). Palynomorph concentrations in Hole 29A tend to decrease upcore, from a mean ~93,600 palynomorphs/cm^3 (range 6700–177,200 palynomorphs/cm^3) in sequence m4.4, ~99,800 palynomorphs/cm^3 in the only sample analyzed from sequence m4.3, and mean ~53,900 palynomorphs/cm^3 (range 15,000–99,800 palynomorphs/cm^3) in sequence m4.2. *Habibacysta tectata* and *Spiniferites* spp. are usually common to abundant in sequences m4.4–m4.2 in Hole 29A, together with common *Batiacasphaera sphaerica* and *Labyrinthodinium truncatum modicum*; *Lingulodinium machaerophorum*. *Labyrinthodinium truncatum truncatum*, and *Trinovantedinium papulum* are also quite consistently present (Figs. 6, 7, and 10; Supplemental Tables 1 and 2 [see footnotes 1 and 2]). The highest common occurrence of several dinocyst taxa occur in these sequences in Hole 29A: *Cleistosphaeridium placacanthum* (sample 29A-85R-2, 99–100 cm, 383.25 mcd), *Labyrinthodinium truncatum modicum* and *Selenopemphix brevispinosa* (sample 29A-75R-1, 41–42 cm, 353.72 mcd), and *Dapsilidinium pseudocolligerum* (sample 29A-74R-2, 57–58 cm, 352.32 mcd; Supplemental Table 2 [see footnote 2]). Like sequence m4.5 and upper sequence m5, these sediments are assigned to DN5b. Acritarchs, particularly the genera *Cyclopsiella* and *Michrystridium* can be common to abundant in these sequences (Supplemental Tables 1 and 2 [see footnotes 1 and 2]), probably recording freshwater flux during the late Langhian.

Lithologic Unit II: Sequence m4.1

Palynological assemblages were very sparse in sequence m4.1 (mean concentration = 29,800, range 9400–50,500 palynomorphs/cm^3, n = 9 in Hole 29A and mean ~20,900, range 8600–45,500 palynomorphs/cm^3, n = 9 in Hole 27A), with mean T:M ~5.06 (range 3.07–10.24, n = 7) in Hole 29A and mean T:M ~7.79 (range 2.63–17.5, n = 7) in the more proximal Hole 27A. The dinocyst assemblage was dominated by long-ranging, ubiquitous taxa, precluding precise age assignments in Hole 27A. Dinocyst assemblages strongly dominated by protoperidinioid cysts such as *Lejeunecysta* spp., *Brigantedinium* spp., *Echinidinium* spp., and *Trinovantedinium papulum* characterize the sediments at both sites, with *Spiniferites* spp., *Batiacasphaera sphaerica*, and *Habibacysta tectata* being the only consistently common gonyaulacoid cysts, although *Hystrichosphaeropsis obscura* is consistently present (Figs. 6 and 7; Supplemental Tables 1 and 2 [see footnotes 1 and 2]). At the more distal Site 29, the LO of *Selenopemphix dionaeacysta* (in sample 29A-70R-1, 107–108 cm, 339.13 mcd) and *Ataxiodinium zevenboomii* (in sample 29A-64R-1, 120–121 cm, 320.96 mcd) occur within sequence m4.1, allowing assignment to DN6 (Fig. 7; Table 2, Supplemental Table 2 [see footnote 2]). This estimate agrees with all other proxies (Browning et al., 2013). The abundance of the acritarch genus *Cyclopsiella* and the consistent presence of *Polyshaperidium zoharyi* are similar to the observations of de Verteuil and Norris (1996) for their *Selenopemphix dionaeacysta* interval zone. Diverse angiosperm-dominated pollen assemblages are characterized by an upsequence decrease in bisaccate pollen grains, paired with an increase in *Carya* (hickory) grains (particularly in Hole 27A; Figs. 3 and 4; Table 6). This records climatic amelioration and/or increasingly neritic conditions. All samples examined from this sequence in Hole 27A are strongly dominated by phytoclasts (palynofacies type 1; mean Ph:AOM = 81.67, range 3.3–124, n = 8). A few samples (e.g., 29A-65R-2, 18–19 cm, 324.50 mcd, and 29A-64R-1, 120–121 cm, 320.96 mcd, from which many of the specimens illustrated in Fig. 10 were identified) at the more distal site were relatively rich in AOM and assigned to palynofacies type 2 of Batten (1996). Ph:AOM values range from 0.11 to 45.75 in sequence m4.1 in Hole 29A (Table 5).

Overall Trends through the Miocene

Terrestrial palynomorphs (pollen and embryophyte spores) outnumber marine algae (dinoflagellates and acritarchs) in all but one sample analyzed in this study (29A-116R-1, 120–121 cm, 473.46 mcd, where T:M = 0.56), reflecting strong terrigenous flux to the New Jersey margin throughout the Miocene. The average T:M through the Miocene in Hole 27A is ~5.4 and ~3.6 in the more distal Hole 29A. Strong peaks in T:M are found sporadically throughout the Miocene in Holes 27A and 29A (Figs. 3–5; Tables 3 and 4), and are frequently in silty muds associated with sequence-bounding unconformities (e.g., m6, m5.7, m5.4, m5.3.3, m5.3, m4.5, and m4.4-m4.1 in Hole 27A, and m5.7, m5.45, m5.4, m4.4, m4.3, m4.2, and m4.1 in Hole 29A) or with palynomorph-rich silty muds within sequences (e.g., ~527, 469, 434, and 194 mcd in Hole 27A and ~575, 549, 529, 457, 440, and 325 mcd in Hole 29A). Transgressive systems tracts (TSTs) (identified by Miller et a., 2013a), in contrast, are characterized by very low T:M, e.g., ~465, 333, 271, 243, and 217 mcd in Hole 27A (where T:M ranges from 1.27 to 2.24)

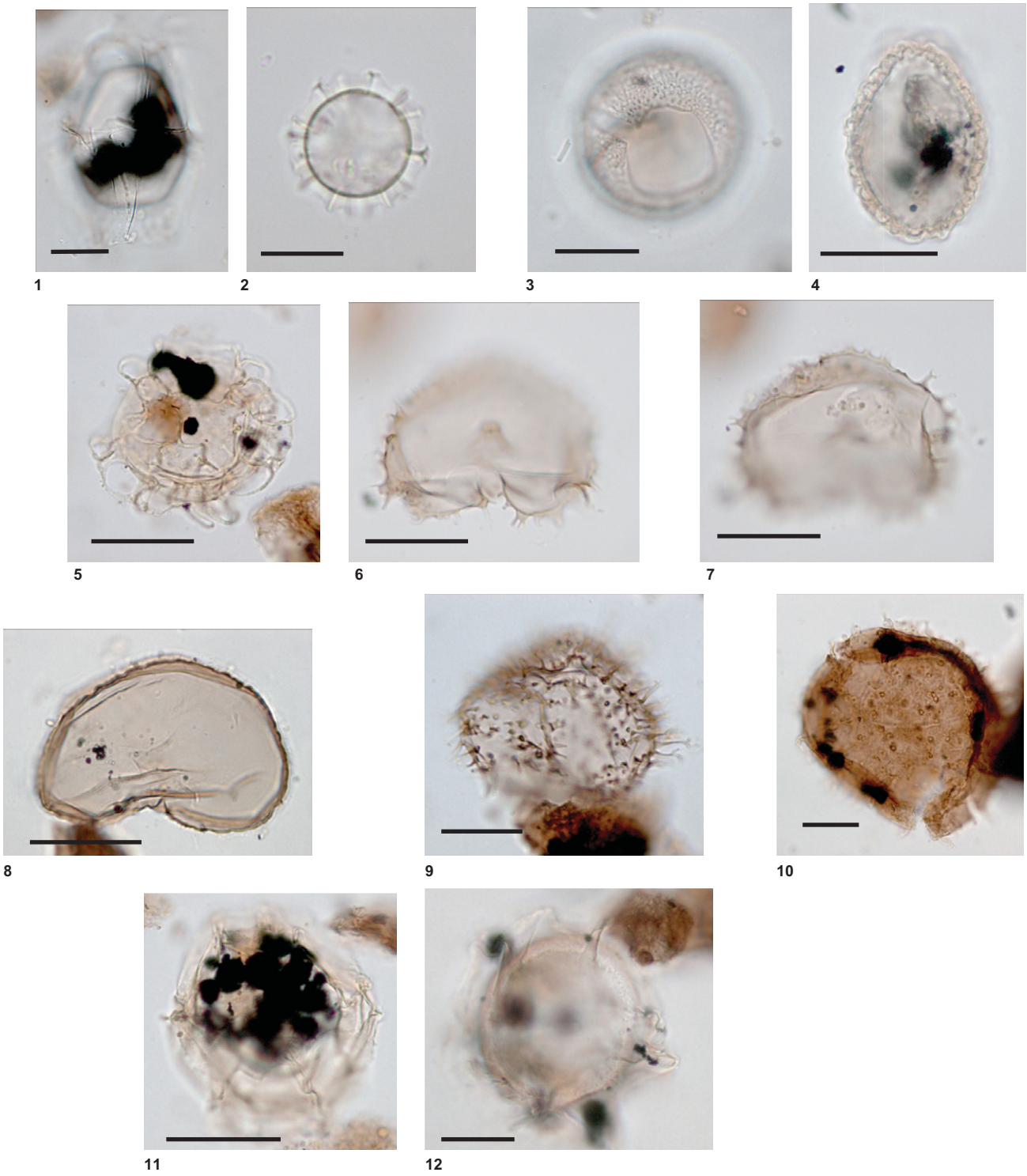

Figure 10. Common marine palynomorphs in sequences m4.5–m4.1 (lower Serravallian, dinoflagellate zones DN5b–DN6) including species, sample number, depth (in parentheses), and England Finder coordinates. (1) *Hystrichosphaeropsis obscura* Habib 1972: 313–29A- 64R-1 (120–121 cm), B61/2. (2) *Labyrinthodinium truncatum* ssp. *truncatum* Piasecki 1980: 313–29A- 64R-1 (120–121 cm), V41/0. (3) *Habibacysta tectata* Head et al. 1989: 313–29A- 64R-1 (120–121 cm), J70/4. (4) *Ataxiodinium zevenboomii*: 313–29A-64R-1 (120–121 cm), X53/4. (5) *Unipontidinium aquaeductum* (Piasecki) Wrenn 1988: 313–29A-92R1 (100–101 cm), M57/0-H33/4-V39/3. (6, 7) *Selenophemphix dionaeacysta* Head et al. 1989: 313–29A- 64R-1 (120–121 cm), J45/3-K44/2. (8) *Selenophemphix brevispinosa* Head et al. 1989: 313–29A- 64R-1 (120–121 cm), B49/4. (9) *Trinovantedinium harpagonium* de Verteuil and Norris 1992: 313–29A-92R1 (100–101 cm), U69/3. (10) *Sumatradinium soucouyantiae* de Verteuil and Norris 1992: 313–29A-92R1 (100–101 cm), G64-3. (11) *Impagidinium arachnion* de Verteuil and Norris 1996: 313–29A-92R1 (100–101 cm), N51/2-M51/4. (12) *Pentadinium laticinctum* Gerlach 1961: 313–29A-64R-1 (120–121 cm), L67/2.

and ~585 mcd in Hole 29A, where T:M = 2.04 (Tables 3 and 4). The oldest strong peak in terrestrial versus marine palynomorphs (T:M = 11.4) is in sample 27A-187R-CC (8–20 cm, 527.68 mcd; Fig. 3), in sequence O6 (earliest Aquitanian). The oldest peak at Site 29 (T:M = 11.82) was in sample 29A-211R-1 (31–32 cm, 737.92 mcd), in sequence m5.8 (Fig. 3), in sediments of Aquitanian–early Burdigalian age. The strongest T:M values in both holes are in sediments of late Burdigalian age (DN3, NN4, and East Coast Diatom Zone ECDZ2) near sequence boundary m5.4; T:M was 43.25 in sample 27A-104R-3 (36–38 cm, 301.86 mcd), near the top of sequence m5.45, and T:M was 12.76 in sample 29A-182R-2 (99–100 cm, 660.81 mcd), ~1.5 m above sequence boundary m5.4.

The ratio of phytoclasts versus AOM (Ph:AOM), which might be expected to record much the same information as T:M, shows much less sample to sample variability upcore at both sites, but shows marked increases in palynodebris of terrestrial origin at particular times. Phytoclasts first outnumber AOM in sequence 5.8 in both holes, but phytoclasts overwhelm AOM (i.e., are assigned to palynofacies type 1 of Batten [1996], rather than type 2, which characterizes most of the earlier Miocene) much earlier at Site 27 than at Site 29. The oldest sample in which phytoclasts outnumber AOM in Hole 27A is sample 27A-169R-1 (32–33 cm, 484.93 mcd, in sequence m5.8), and the earliest strong dominance of phytoclasts (Ph:AOM > 5) is in sample 27A-164R-2 (61–62 cm, 471.47 mcd, also in sequence m5.8). There is a dramatic increase (Ph:AOM > 40) in the Ph:AOM in sample 27A-105R-CC (301.61 mcd), near the top of sequence m5.45 (Fig. 3). In Hole 29A, phytoclasts first outnumber AOM in sample 29A-210R-3 (18–19 cm, 737.74 mcd, in sequence m5.8) and Ph:AOM first exceeds 5 in sample 29A-157R-2 (20–21 cm, 589.86 mcd, near the base of sequence m5.2; Fig. 4). The first dramatic increase in Ph:AOM in Hole 29A occurs in sample 29A-98R-2 (70–71 cm, 421.26 mcd in sequence m4.5; Fig. 3). The Ph:AOM signal at the two sites is nearly identical above sequence m4.5, suggesting that the shelf had prograded past Site 29 by the latest Langhian–early Serravallian (Fig. 5).

Nonsaccate (mainly angiosperm) pollen outnumber bisaccate conifer pollen in nearly every sample analyzed from both holes (Figs. 3 and 4; Table 6), with exceptions in Hole 27A in samples 190R-3 (15–16 cm, 536.54 mcd), 190R-2 (119–120 cm), 189R-1 (72–73 cm, 531.08 mcd), 188R-2 (60–61 cm, 529.21 mcd; in sequence O6), 166R-1 (15–16 cm, 475.62 mcd), 165R-1 (115–116 cm, 473.16 mcd), 164R-2 (110–111 cm, 470.46 mcd; in sequence m5.8), and 88R-2 (110–111 cm, 252.86 mcd; at the base of sequence m5.2), and in Hole 27A in samples 211R-2 (24–25 cm, 739.35 mcd), 211R-1 (31–32 cm, 737.92 mcd), 209R-1 (111–112 cm, 732.62 mcd; in sequence m5.8), 190R-1 (130–131 cm; in sequence m5.47), and 129 R-1 (89–90 cm, 509.75 mcd; in sequence m5.2). Nonsac:bisac first exceeds 10:1 in sample 27A-170R-1 (51–52 cm, 488.17 mcd, in sequence m5.8) and in sample 29A-207R-3 (728.51 mcd, in sequence m5.7). The nonsac:bisac pollen ratio increases sharply in sequence m5.8 in Hole 27A and remains relatively high until sequences m5.4–m5.33. Following a peak in upper sequence m5.3, the nonsac:bisac ratio declines again in sequences m5.2–m4.2, then rise sharply in sequence m4.1 (Fig. 3). In Hole 29A, nonsac:bisac pollen ratio peaks around sequence boundary m5.7 and is high in sequence m5.45, sequences m5.3–m5.2, and again in sequence m4.4 (Fig. 4).

Terrigenous palynomorphs tend to increase in relative and absolute concentrations (high T:M and high pollen/spore concentrations) in proximity to sequence boundaries. The palynological signatures near sequence boundaries are indicative of increased proximity to the shoreline and/or more neritic conditions as well as the greater resistance of pollen and spores (evolved for wind pollination) to oxidation than dinoflagellate cysts. The ratio of more oxidation-resistant gonyaulacoid cysts versus more susceptible protoperidinioid cysts (G:P) tends to be high in the lower parts of sequences where terrestrial palynomorph abundances are low (Figs. 3 and 4; Tables 3 and 4), recording low rates of sediment accumulation in TSTs, probably due to higher accommodation and/or more distal settings in TSTs (as discussed in McCarthy et al., 2003; Gostlin, 1999). High concentrations of terrestrial palynomorphs in the upper parts of sequences record aggradation and progradation within the sequences. Protoperidinioids can also be very rare within dinocyst-rich sequences, such as in samples 27A-187R-3 (140–141 cm), 27A-187R-1 (87–88 cm; 526.08–523.57 mcd in sequence O6), where G:P values were 8.33 and 9.00, respectively, 29A-170R-2 (630.82 mcd in sequence m5.3), and 29A-109R-2 (20–21 cm, 452.61 mcd in sequence m4.5), where G:P values were 15.33 and 13.00, respectively (Figs. 3 and 4; Tables 3 and 4).

RELATIVE SEA-LEVEL RECONSTRUCTIONS COMPARED WITH GLACIOEUSTASY

The relationship between sea level and the palynological assemblage is more complex than that with the benthic foraminiferal assemblage, which is largely a function of paleo–water depth due to changes in physiochemical parameters that vary with water depth (Katz et al., 2013). Most of the palynological samples examined from IODP Expedition 313 contain more allochthonous than authochthonous elements, and thus cannot reflect the local depositional environment, as do the foraminiferal assemblages. In addition to variations in sea surface productivity, T:M reflects variations in the numerous mechanisms that transport pollen and embryophyte spores to each offshore site, i.e., wind, rivers, ocean currents, and mass transport, most of which are related to distance from the shoreline. High sea surface productivity can be inferred from the abundance of round-brown dinoflagellate cysts, *Brigantedinium* spp. (Zonneveld et al., 2001, 2008; Versteegh and Zonneveld, 2002), and the abundance of AOM derived from algal decomposition (Batten, 1996). The relative importance of wind can be estimated by examining the relative abundance of bisaccate pollen (Mudie and McCarthy, 1994). The influence of rivers can be identified lithologically (e.g., in sequence m5.8; Miller et al., 2013a) as well as by large pulses of acritarchs. Mass transport is largely restricted to environments on clinoform bottomsets (e.g., much of the Early to Middle Miocene at Site M29; Mountain et al., 2010) and to continental slope and rise sediments (McCarthy and Mudie, 1998). Following progradation of the clinoform break past a site, downslope transport would no longer play a significant role, but until then, recycling and resedimentation of palynomorphs from the shelf would have been a major overprint to our records. This is evident in the continental margin architecture (Fig. 5): Hole 27A is continuously neritic above lithologic unit VI (sequence m5.8), so mass wasting would have been far less important at this site after the early Burdigalian. By the middle Burdigalian, the overwhelming dominance of phytoclasts in the palynofacies and very sparse AOM (Figs. 3–7) record a very strong terrigenous component in the majority of samples analyzed in lithological units III and II. Ph:AOM shows less variability through the Miocene at each site than the ratio of terrestrial versus marine palynomorphs. Peaks in T:M in AOM-rich sediments thus record pulses of terrigenous flux into deep-water settings, mainly via mass wasting (e.g., in sequence m5.8 in Hole 27A and in sequences m5.3–m5.2 in Hole 29A), whereas high T:M in phytoclast-rich sediments records sedimentation in neritic settings.

Because the palynofacies primarily reflects distance from the shoreline, and foraminiferal assemblages largely reflect the paleo–water depth, the response of palynological and

benthic foraminiferal assemblages to sea-level change will differ, depending on the gradient of the margin and the position of the rollover. Whereas the resolution available with foraminiferal estimates of sea level cannot discriminate sea-level lowerings of a few tens of meters, an increase in terrigenous flux recorded by high T:M can record downslope mass wasting from neritic environments into relatively deep water environments in response to regression. Subsequent onlapping sequences (e.g., m5.7, m5.3, m5, m4.4–m4.2) are characterized high AOM except around seismic sequence boundaries, suggesting taphonomic effects associated with the generation of sequence boundaries (e.g., resedimentation, selective oxidation; cf. McCarthy et al., 2003). In addition, the much lower gradient of the margin once the clinoform has prograded past a site (past Site 27 during the late Burdigalian DN3 [18. 1–15.97 Ma], marked by Ph:AOM = 102 in sample 27A-105R-CC [301.61 mcd], and past Site 29A during the latest Langhian, ca. 14.2–13.2 Ma, DN5b recorded by Ph:AOM = 40.4 in sample 29A-98R-2 [70–71 cm, 421.26 mcd; Table 5]) results in much more proximal palynological assemblages (high T:M, Ph:AOM, nonsac:bisac) relative to foraminiferally derived paleobathymetric estimates (Figs. 3–5; Tables 3–6).

Distal deep-water settings were thus inferred whenever multiple palynological proxies concur, i.e., low T:M (Figs. 3–5)/ high M:T (Figs. 11A, 11B), low nonsac:bisac pollen ratios (Figs. 3 and 4; Table 6), low phytoclasts versus AOM (Ph:AOM in Figs. 3–5; Table 5), as well as high G:P (Figs. 3 and 4; Tables 3 and 4), and where upper middle neritic (50–80 m; *Bulimina gracilis*/*Bolivina paula*–dominated biofacies), outer middle neritic (75–100 m; *Uvigerina* spp./*Bolivina floridana*–dominated biofacies), or outer neritic (>100 m; high-diversity, low-dominance assemblages with key indicator taxa, e.g., *Cibicidoides pachyderma*, *Hanzawaia mantaensis*, and *Oridorsalis umbonatus*) water depths were indicated by the foraminiferal assemblages (Mountain et al., 2010; Katz et al., 2013) (Figs. 11A, 11B). As previously observed (McCarthy et al., 2003), the primary ecological signal is confounded by strong taphonomic skewing at sequence boundaries, preferentially degrading neritic protoperidinioid dinoflagellate cysts and thin-walled pollen.

Taking these caveats into consideration, there is generally good agreement between palynologically based estimates of position of the shoreline (and shelf break) and foraminiferally derived paleobathymetric estimates (Figs. 11A, 11B). This allowed us to qualitatively reconstruct relative sea level at each site with some degree of confidence (Figs. 11A, 11B). The interpretation of high terrigenous flux as typically recording low sea levels is consistent with the shallow paleodepths usually reconstructed based on the benthic foraminiferal assemblages in pollen-rich sediments, which are *Hanzawaia concentrica*–dominated biofacies (interpreted as middle inner neritic, 10–25 m) (Katz et al., 2013). Samples rich in nonsaccate pollen that tends to preferentially settle in coastal and inner neritic environments (Mudie and McCarthy, 1994; McCarthy et al., 2003) support the interpretation of a middle inner neritic depositional environment. Increased proximity to the shoreline at times of lower sea level would also tend to decrease the ratio of marine versus terrestrial palynomorphs (M:T in Figs. 11A, 11B) due to ecological stress on marine phytoplankton in inner neritic environments.

The sea-level reconstructions also appear to be consistent with other available data from IODP Expedition 313. Proximal low sea-level settings are generally suggested by very terrigenous samples at sequence boundaries (Figs. 11A, 11B), and strong taphonomic alteration in these sediments is also recorded by high G:P (Figs. 3 and 4). The reconstructions of coastal to inner neritic paleodepths at most sequence boundaries correlate with times of medium to major sea-level lowering according to the compilation of Snedden and Liu (2010). The identification of TSTs and maximum flooding surfaces (MFS) at very high relative sea level (Tables 3 and 4; Figs. 11A, 11B), in contrast, is consistent with our interpretation of distal deep-water environments (Miller et al., 2013a; Browning et al., 2013).

The combination of the two relative sea-level proxies provides more information than either in isolation. For example, the sudden deepening is evident in our sea-level reconstructions during the early Langhian (in sediments assigned to DN4, NN4, and ECDZ2). Outer middle neritic (75–100 m) and outer neritic (>100 m) paleodepth estimates for sequences m5.3 through m5 at Sites 27 and 29, respectively, are paired with quite variable reconstructions of terrigenous flux derived from the palynofacies, recording the rapid aggradation and progradation of lithologic unit II into relatively deep water environments. The interpretation of deep water is consistent with the low deep-sea oxygen isotope values of the Middle Miocene Climate Optimum (Zachos et al., 2001; see fig. 7 in Browning et al., 2013). Similarly, both sets of proxies record a rapid sea-level fall during the late Langhian that correlates with event Mi3 (in sediments assigned to DN5b, NN5, and ECDZ6a-b; Figs. 11A, 11B). One advantage of the palynological approach in reconstructing relative sea level is that palynomorphs and palynodebris were available in statistically significant quantities in more samples than were benthic foraminifers, particularly at the more inner to middle neritic Site 27. This higher resolution record allowed the identification of possible parasequences within thick sequences in both holes. The accumulation of nearly 200 m of sediment beyond the paleoclinoform break in Hole 29A during the early–middle Langhian allows two high-amplitude and 11 lower amplitude sea-level cycles to be identified in sequences m5.3–m5 (Fig. 11B). The dinocyst zonation suggests that these sequences were deposited between 15.97 and 14.2 Ma (zones DN4–DN5a), which agrees well with the estimate of ca. 16.1–14.6 Ma based on the compilation of all chronostratigraphic proxies (by Browning et al., 2013). The resulting periodicity estimates (~136–160 k.y.) in our relative sea-level curves suggest possible Milankovitch forcing, although the chronological control is not sufficient to demonstrate this conclusively; in Miller et al. (2013b), 8 flooding surfaces (including the MFS) were noted in sequence m5.2 at Hole M29A, similar to the 7–8 noted here (Fig. 11B) within the ~1 m.y. of this sequence (15.6–14.6 Ma; Browning et al., 2013). We also note that there are 6–7 flooding events in the Hole M29A m4.5–m4.1 section, which represents ca. 13.6 to ca. 13.0 Ma (Fig. 11B; Browning et al., 2013). The chronology is not sufficient to establish that these are actually quasi-100-k.y.-scale events, but the general match is intriguing.

Given the available resolution, with chronological control provided by multiple biostratigraphic proxies and by Sr isotope ages (Browning et al., 2013), we were able to correlate all of the Mi events shown in figure 7 of Browning et al. (2013) with intervals of lowered sea level reconstructed from the integrated palynological and foraminiferal proxies. These observations, together with the palynological evidence of accelerated offshore sediment transport at times of lowered sea level, and associated progradation and downslope mass wasting, suggest that eustasy is an important factor influencing the architecture of the New Jersey margin.

CONCLUSIONS

A comparison of paleo–water depth estimates inferred from benthic foraminifera (Katz et al., 2013) and distance from shoreline estimates derived from the palynological data allowed relative sea level to be qualitatively reconstructed in Holes 27A and 29A on the New Jersey margin. Although qualitative, this simple estimate

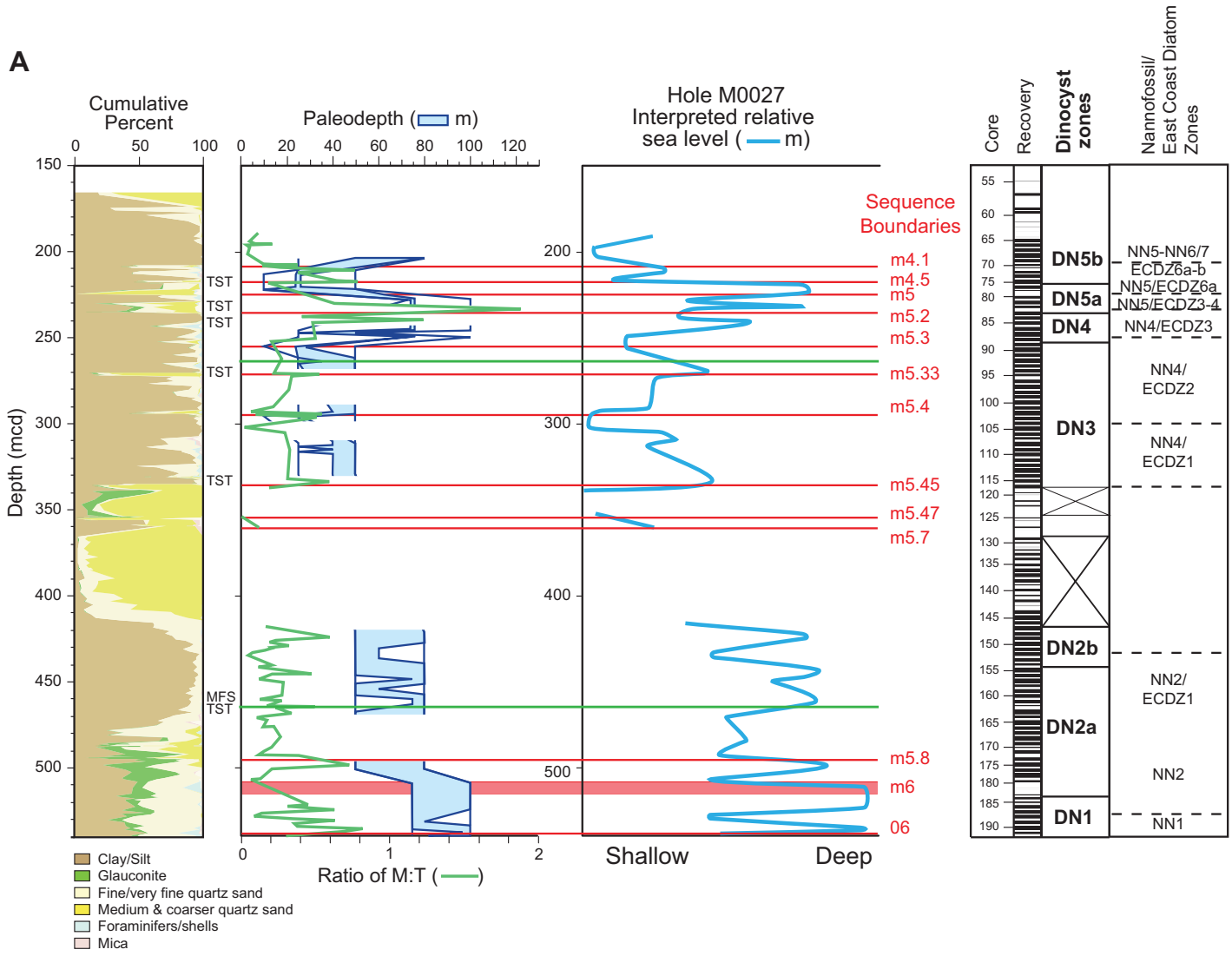

Figure 11 (*on this and following page*). Relative sea level was qualitatively reconstructed by combining paleodepth estimates derived from benthic foraminiferal assemblages (blue, left) and distance from shoreline estimates derived from the ratio of marine versus terrestrial (M:T) palynomorphs (green, left). Depth: mcd—meters composite depth. (A) Integrated Ocean Drilling Program Hole 27A. Sequence boundaries (m6–m4.1) are associated with very low relative sea level, whereas maximum flooding surfaces (MFS) and transgressive surfaces (TS) are associated with foraminiferal and palynological proxies recording high relative sea level. Our sea-level interpretation also appears to identify parasequences, such as in the thick sequence m5.8 in Hole 27A and m5.2 in Hole 29A. Age control is provided by dinocyst zones, together with calcareous nannofossil and diatom zone assignments and Sr isotope age estimates from Browning et al. (2013), allowing intervals of very low sea level to be correlated with Miocene oxygen isotope (Mi) events (see Browning et al., 2013, fig. 7). These generally correlate with the sequence boundaries identified across the New Jersey shallow shelf, supporting the contention that relative sea-level change and the architecture of the New Jersey margin are primarily responses to eustasy.

of relative sea-level change provides a useful framework with which other variations at the IODP Expedition 313 drill sites can be compared. Further, the simple estimate represents a good starting point for subsequent work on eustatic reconstructions, which require backstripping to account for compaction, loading and/or flexure, and thermal subsidence. Our data-based reconstruction can be compared with ongoing modeling studies.

High terrigenous flux associated with fluvial discharge and/or progradation of the New Jersey shelf is recorded by peak concentrations of pollen rich in angiosperm taxa and phytoclasts in sediments deposited in very shallow water or redeposited downslope from coastal and/or upper neritic to middle inner neritic environments, based on paleodepth estimates from benthic foraminiferal assemblages. The low sea levels are interpreted where sediments are rich in angiosperm pollen and phytoclasts and foraminifer samples are either barren, almost completely dominated by *Lenticulina* spp., or assigned to the *Hanzawaia concentrica*–dominated biofacies.

The dinocyst zonation of de Verteuil and Norris (1996) allowed ages to be assigned to all Miocene sequences recovered from Holes 27A and 29A. Additional chronostratigraphic control was provided by calcareous nannofossils and

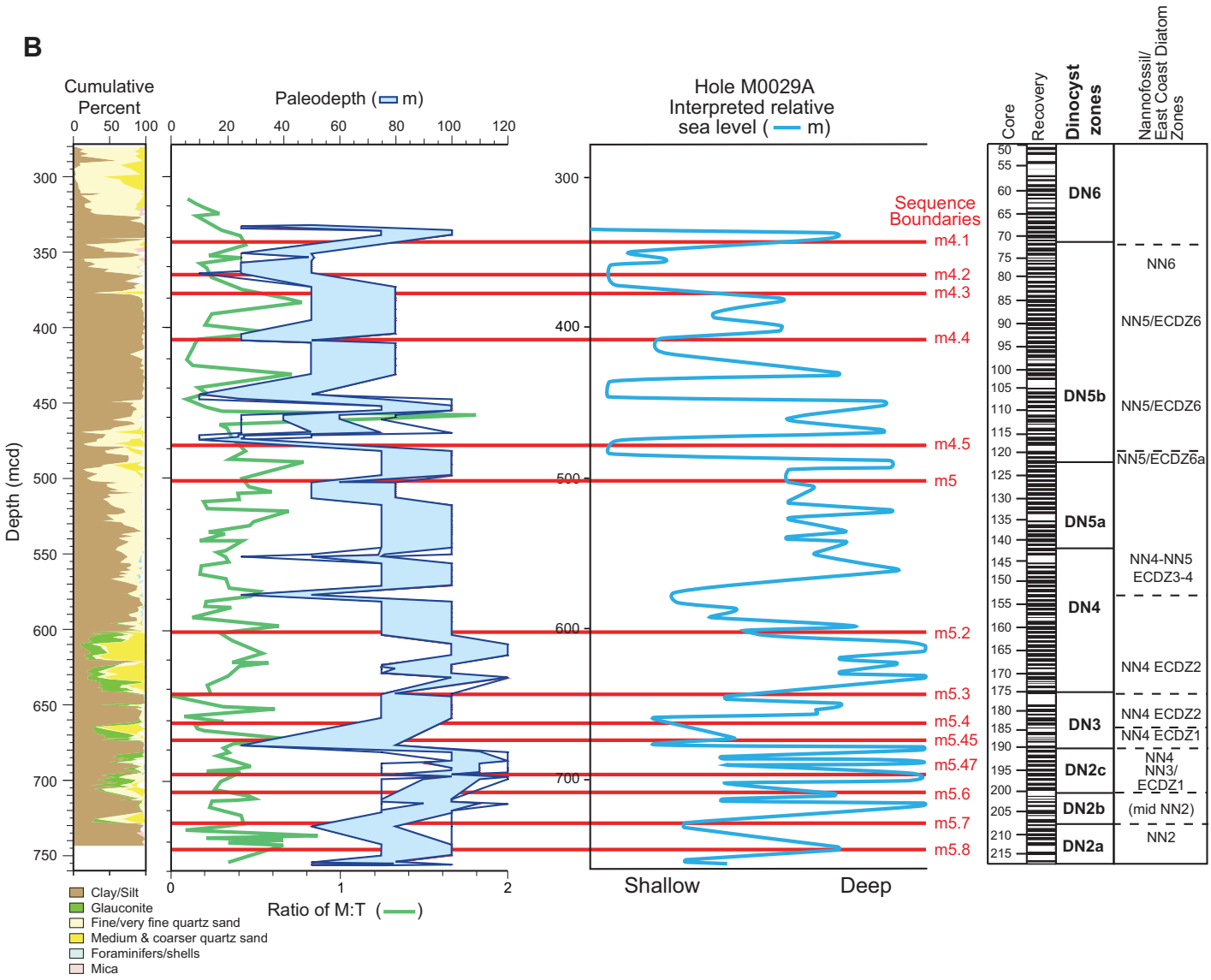

Figure 11 (*continued*). (B) Hole 29A.

diatoms, as well as by Sr isotope pages (Browning et al., 2013) allowing sequence boundaries generated at times of lowered sea level to be correlated with Miocene oxygen isotope events. In contrast, distal environments are recorded by low T:M (high M:T) and a dominance of AOM in onlapping sequences m5.7–m5.6 (early Burdigalian), m5.3–m5 (Langhian), and m4.4 (latest Langhian–earliest Serravallian). High sea level at these times is recorded by benthic foraminiferal assemblages indicative of lower middle to outer neritic environments. This study illustrates the value of palynology in sequence stratigraphic studies, and of combining palynological and benthic foraminiferal proxies to produce robust reconstructions of relative sea level and relate these to sedimentation on continental margins.

ACKNOWLEDGMENTS

We acknowledge the input of the entire Integrated Ocean Drilling Program (IODP) Expedition 313 Scientific Party and the IODP staff in Bremen, and current and former students and colleagues in the Palynology Lab at Brock University: E. Fischer, S. Tiffin, J. Hopkins, K. Gostlin, M. Mahdavi, M. Head, and K. Sihra. Mike Lozon provided invaluable assistance with drafting. This research used samples and/or data provided by the IODP and the International Continental Scientific Drilling Program (ICDP). Funding for this research was provided by a Natural Sciences and Engineering Research Council of Canada (NSERC) Discovery Grant to McCarthy, NSERC Undergraduate Student Research Awards to Zanatta and Drljepan, U.S. Science Support Program and National Science Foundation awards (Browning, Katz, Miller, and Mountain), and by the German Science Foundation (DFG project KO 3944/3-1 to Kotthoff). We thank two anonymous reviewers and editor Carol Frost for their helpful comments on an earlier draft of our paper, and especially guest editor Jean-Noel Proust, who meticulously edited the revised draft of this paper.

REFERENCES CITED

Austin, J.A., Jr., and 28 others, 1998, Proceedings of the Ocean Drilling Program, Initial reports, Volume 174A: College Station, Texas, Ocean Drilling Program, doi: 10.2973/odp.proc.ir.174a.1998.

Batten, D.J., 1996, Palynofacies, *in* Jansonius, J., and McGregor, D.C., eds., Palynology: Principles and applications: American Association of Stratigraphic Palynologists Foundation, v. 3, p. 1011–1084.

Browning, J.V., Miller, K.G., Barron, J., Sugarman, P.J., McCarthy, F.M.G., Kulhanek, D., Katz, M.E., and Feigenson, M.D., 2013, Chronology of Oligocene–Miocene sequences, onshore and nearshore New Jersey: Implications for regional, interregional, and global correlations: Geosphere, v. 9, doi:10.1130/GES00857.1.

de Verteuil, L., and Norris, G., 1996, Miocene dinoflagellate stratigraphy and systematics of Maryland and Virginia: Micropaleontology: Supplement, v. 42: New York, Micropaleontology Press, 172 p.

Dybkjær, K., and Piasecki, S., 2008, A new Neogene biostratigraphy of Denmark: Geological Survey of Denmark, Greenland Bulletin 15, p. 29–32.

Dybkjær, K., and Piasecki, S., 2010, Neogene dinocyst zonation for the eastern North Sea basin, Denmark: Review of Palaeobotany and Palynology, v. 161, p. 1–29, doi: 10.1016/j.revpalbo.2010.02.005.

Eshet, Y., Druckman, Y., Cousminer, H.L., Habib, D., and Drugg, W.S., 1988, Reworked palynomorphs and their use in the determination of sedimentary cycles: Geology, v. 16, p. 662–665, doi:10.1130/0091-7613(1988)016<0662:RPATUI>2.3.CO;2.

Gostlin, K.E., 1999, Continental margin architecture: the palynological signature of glacioeustasy [M.S. thesis]: St. Catharines, Canada, Brock University, 160 p.

Gradstein, F., Ogg, J., and Smith, A., 2004, A geologic time scale 2004: Cambridge, U.K., Cambridge University Press, 589 p.

Gregory, W.A., and Hart, G.F., 1992, Towards a predictive model for the palynologic response to sea level changes: Palaios, v. 7, p. 3–33, doi:10.2307/3514794.

Habib, D., and Miller, J.A., 1989, Dinoflagellate species and organic facies evidence of marine transgression and regression in the Atlantic Coastal Plain: Palaeogeography, Palaeoclimatology, Palaeoecology, v. 74, p. 23–47, doi:10.1016/0031-0182(89)90018-7.

Hopkins, J.A., and McCarthy, F.M.G., 2002, Post-depositional palynomorph degradation in Quaternary shelf sediments: A laboratory experiment studying the effects of progressive oxidation: Palynology, v. 26, p. 167–184, doi:10.1080/01916122.2002.9989571.

Katz, M.E., Miller, K.G., and Mountain, G.S., 2003, Biofacies and lithofacies evidence for paleoenvironmental interpretations of upper Neogene sequences in the New Jersey continental shelf (ODP Leg 174A), *in* Olson, H.C., and Leckie, R.M., eds., Micropaleontologic proxies for sea-level change and stratigraphic discontinuities: SEPM (Society for Sedimentary Geology) Special Publication 75, p. 131–146, doi:10.2110/pec.03.75.0131.

Katz, M.E., Browning, J.V., Miller, K.G., Monteverde, D., Mountain, G.S., and Williams, R.H., 2013, Paleobathymetry and sequence stratigraphic interpretations from benthic foraminifera: Insights on New Jersey shelf architecture, IODP Expedition 313: Geosphere, doi:10.1130/GES00872.1.

Louwye, S., and Laga, P., 2008, Dinoflagellate cyst stratigraphy and paleoenvironment of the marginal marine Middle and Upper Miocene of the eastern Campine area, northern Belgium (southern North Sea basin): Geological Journal, v. 43, p. 75–94, doi:10.1002/gj.1103.

Martini, E., 1971, Standard Tertiary and Quaternary calcareous nannoplankton zonation, *in* Farinacci, A., ed., Proceedings of the Second International Conference on Planktonic Microfossils 1970, Volume 2: Rome, Edizioni Tecnoscienza, p. 739–785.

McCarthy, F.M.G., and Gostlin, K.E., 2000, Correlating Pleistocene sequences across the New Jersey margin: Sedimentary Geology, v. 134, p. 181–196, doi: 10.1016/S0037-0738(00)00019-1.

McCarthy, F.M.G., and Mudie, P.J., 1998, Oceanic pollen transport and pollen:dinocyst ratios as markers of late Cenozoic sea level change and sediment transport: Palaeogeography, Palaeoclimatology, Palaeoecology, v. 138, p. 187–206, doi:10.1016/S0031-0182(97)00135-1.

McCarthy, F.M.G., Gostlin, K.E., Mudie, P.J., and Hopkins, J.A., 2003, Terrestrial and marine palynomorphs as sea-level proxies: An example from Quaternary sediments on the New Jersey Margin, U.S.A., *in* Olson, H.C., and Leckie, R.M., eds., Micropaleontologic proxies for sea-level change and stratigraphic discontinuities: SEPM (Society for Sedimentary Geology) Special Publication 75, p. 119–129, doi:10.2110/pec.03.75.0119.

McCarthy, F.M.G., Gostlin, K.E., Mudie, P.J., and Ohlenschlager, R., 2004a, The palynological record of terrigenous flux to the deep sea: Late Pliocene–recent examples from 41°N in the abyssal Atlantic and Pacific Oceans: Review of Palaeobotany and Palynology, v. 128, p. 81–95, doi:10.1016/S0034-6667(03)00113-1.

McCarthy, F.M.G., Findlay, D.J., and Little, M.L., 2004b, The micropaleontological character of anomalous calcareous sediments of late Pliocene through early Pleistocene age below the CCD in the northwest North Pacific: Palaeogeography, Palaeoclimatology, Palaeoecology, v. 215, p. 1–15, doi:10.1016/j.palaeo.2004.07.032.

Miller, K.G., 2002, The role of ODP in understanding the causes and effects of global sea-level change: JOIDES Journal, v. 28, p. 23–28.

Miller, K.G., Rofolo, S., Sugarman, P.J., Pekar, S.F., Browning, J.V., and Gwynn, D.W., 1997, Early to middle Miocene sequences, systems tracts, and benthic foraminiferal biofacies, New Jersey coastal plain, *in* Miller, K.G., and Snyder, S.W., Proceedings of the Ocean Drilling Program, Scientific Results, Volume 150X: College Station, Texas, Ocean Drilling Program, p. 169–186.

Miller, K.G., Kominz, M.A., Browning, J.V., Wright, J.D., Mountain, G.S., Katz, M.E., Sugarman, P.J., Cramer, B.S., Christie-Blick, N., and Pekar, S.F., 2005, The Phanerozoic record of global sea-level change: Science, v. 310, p. 1293–1298, doi:10.1126/science.1116412.

Miller, K.G., Browning, J.V., Mountain, G.S., Bassetti, M.A., Monteverde, D., Katz, M.E., Inwood, J., Lofi, J., and Proust, J.-N., 2013a, Sequence boundaries are impedance contrasts: Core-seismic-log integration of Oligocene–Miocene sequences, New Jersey shallow shelf: Geosphere, v. 9, doi:10.1130/GES00858.1.

Miller, K.G., and 13 others, 2013b, Testing sequence stratigraphic models by drilling Miocene foresets on the New Jersey shallow shelf: Geosphere, v. 9, doi: 10.1130/GES00884.1.

Monteverde, D.H., 2008, Sequence stratigraphic analysis of early and middle Miocene shelf progradation along the New Jersey margin [Ph.D. thesis]: New Brunswick, New Jersey, Rutgers University, 247 p.

Monteverde, D.H., Mountain, G.S., and Miller, K.G., 2008, Early Miocene sequence development across the New Jersey margin: Basin Research, v. 20, p. 249–267, doi: 10.1111/j.1365-2117.2008.00351.x.

Mountain, G., and Monteverde, D., 2012, If you've got the time, we've got the depth: The importance of accurate core-seismic correlation: American Geophysical Union Fall Meeting, abs. PP51B–2111.

Mountain, G.S., Proust, J.-N., McInroy, D., Cotterill, C., and the Expedition 313 Scientists, 2010, Proceedings of the Integrated Ocean Drilling Program, Volume 313: Tokyo, Integrated Ocean Drilling Program Management International, Inc., doi:10.2204/iodp.proc.313.2010.

Mudie, P.J., and McCarthy, F.M.G., 1994, Pollen transport processes in the western North Atlantic: Evidence from cross-margin and north-south transects: Marine Geology, v. 118, p. 79–105, doi:10.1016/0025-3227(94)90114-7.

Oboh-Ikuenobe, F.E., Obi, C.G., and Jaramillo, C.A., 2005, Lithofacies, palynofacies, and sequence stratigraphy of Paleogene strata in southeastern Nigeria: Journal of African Earth Sciences, v. 41, p. 79–101, doi: 10.1016/j.jafrearsci.2005.02.002.

Rochon, A., de Vernal, A., Turon, J.-L., Matthiessen, J., and Head, M.J., 1999, Distribution of recent dinoflagellate cysts in surface sediments from the North Atlantic Ocean and adjacent seas in relation to sea-surface parameters: American Association of Stratigraphic Palynologists Contribution 35, 152 p.

Snedden, J.W., and Liu, C., 2010, A compilation of Phanerozoic sea-level change, coastal onlaps and recommended sequence designations: American Association of Petroleum Geologists Search and Discovery Article 40594, www.searchanddiscovery.com.

Stockmarr, J., 1971, Tablets with spores used in absolute pollen assessment: Pollen et Spores, v. 13, p. 615–621.

Traverse, A., ed., 1994, Sedimentation of organic particles: New York, Cambridge University Press, 544 p.

Tyson, R., 1995, Sedimentary organic matter: Organic facies and palynofacies: London, Chapman & Hall, 615 p.

Versteegh, G.J.M., and Zonneveld, K.A.F., 2002, Use of selective degradation to separate preservation from productivity: Geology, v. 30, p. 615–618, doi:10.1130/0091-7613(2002)030<0615:UOSDTS>2.0.CO;2.

Wood, S.W., and Gorin, G.E., 1998, Sedimentary organic matter in distal clinoforms of Miocene slope sediments: Site 903 of ODP Leg 150, offshore New Jersey: Journal of Sedimentary Research, v. 68, p. 856–868, doi:10.2110/jsr.68.856.

Zachos, J.C., Pagani, M., Sloan, L.C., Thomas, E., and Billups, K., 2001, Trends, rhythms, and aberrations in global climate 65 Ma to present: Science, v. 292, p. 686–693, doi:10.1126/science.1059412.

Zonneveld, K.A.F., Versteegh, G.J.M., and de Lange, G.J., 1997, Preservation of organic walled dinoflagellate cysts in different oxygen regimes: A 10,000 years natural experiment: Marine Micropaleontology, v. 29, p. 393–405, doi:10.1016/S0377-8398(96)00032-1.

Zonneveld, K.A.F., Versteegh, G.J.M., and de Lange, G.J., 2001, Palaeoproductivity and postdepositional aerobic organic matter decay reflected by dinoflagellate cyst assemblages of the Eastern Mediterranean S1 sapropel: Marine Geology, v. 172, p. 181–195, doi: 10.1016/S0025-3227(00)00134-1.

Zonneveld, K.A.F., Versteegh, G.J.M. and Kodrans-Nsiah, M., 2008, Preservation and organic chemistry of late Cenozoic organic-walled dinoflagellate cysts: A review: Marine Micropaleontology, v. 86, p. 179–197.